CHAPTER 5
Co-DOPED TiO_2 THIN FILMS: RESULTS AND DISCUSSION

5.1 Introduction

Thin films of Co-doped TiO_2 are used in a variety of optoelectronic devices due to their high transparency in the visible region of the photonic spectrum combined with a high conductivity. On the other hand, as described in Chapter 3 (Pulsed Laser Deposition of Oxides), PLD is an unique deposition technique in the sense that stoichiometric, multicomponent oxide films can be deposited on substrates even at rather low substrate temperatures without the need for post-annealing treatments. However, the properties of the deposited films are, in general, sensitive to the specific process parameters during film growth.

In this chapter it is demonstrated how properties of the Co-doped TiO_2 films are related to key parameters of the PLD process such as laser output energy, total pressure, substrate temperature, and gaseous atmosphere of either argon or argon and hydrogen. The effect of every parameter is described in a separate section; a detailed description of the experimental conditions is followed by a presentation and discussion of the main results with respect to the influence of the given parameter on the film's crystallographic structure, optical properties, surface microstructure and composition, and electrical and magnetic properties. The overall conclusions of the parametric study are presented in a separate (last) chapter.

5.2 Effect of laser energy density (I)

Laser energy density, or laser fluence is one of the most important parameters governing film properties. Therefore, accurate laser energy and spot area measurements are vital for reproducible film growth.

In this section, the influence of laser energy density on the crystallographic structure and optical properties of the deposited films are discussed.

Films were grown using the PLD deposition system described previously in Chapter 4. The

experiments were performed in an Ar environment at various laser output energies within the range of 52 to 195 mJ for a substrate temperature of 250 ºC, and from 52 to 157 mJ for a substrate temperature of 310 ºC. These values of the laser output energy lead to a calculated laser fluence ranging from 2.1 to 7.9 J/cm^2, according to the description given in Chapter 4. Films were grown for dwell times varying between 50 and 150 minutes, at a laser pulse repetition rate of 20 Hz. The deposition conditions are summarized in Table 5.1.

Table 5.1 PLD parameters and deposition rate of the thin films.

Sample	Laser output energy (mJ)	F (J/cm^2)	T_S (ºC)	P_T (mbar)	Φ_{Ar} (sccm)	No. of pulses	Thickness (nm) [(a)]	Thickness /pulse (Å/pulse)
F55	52	2.1	250	5.0×10^{-1}	30	60 000	–	–
F53	95	3.7				60 000	296	0.050
F65	126	5.1				120 000	992	0.083
F43	157	6.4				60 000	493	0.082
F64	157	6.4				120 000	1800	0.150
F48	157	6.4				60 000	368	0.061
F47	195	7.9				60 000	520	0.087
F46	52	2.1	310			60 000	205	0.034
F57	53	2.2				180 000	683	0.038
F54	95	3.7				60 000	340	0.056
F58	95	3.7				120 000	842	0.070
F45	126	5.1				60 000	612	0.102
F42	157	6.4				60 000	800	0.133
F59	157	6.4				60 000	–	

[(a)] thickness values were obtained by optical transmission

Crystallographic structure

Figure 5.1 displays the XRD patterns of the films obtained at a low substrate temperature of T_S = 250 ºC for varying laser output energy. At low values of the laser fluence, e.g. 2.1 J/cm^2 (sample F55), no crystalline phase – either TiO_2 anatase, rutile or brookite was noticed. Samples F53 and F65 which were prepared at higher laser output energies and consequently higher fluences, 3.7 and 5.1 J/cm^2 respectively, display XRD spectra similar to that of sample F55, although the thickness of deposited material was higher, giving a higher volume of analysed material.

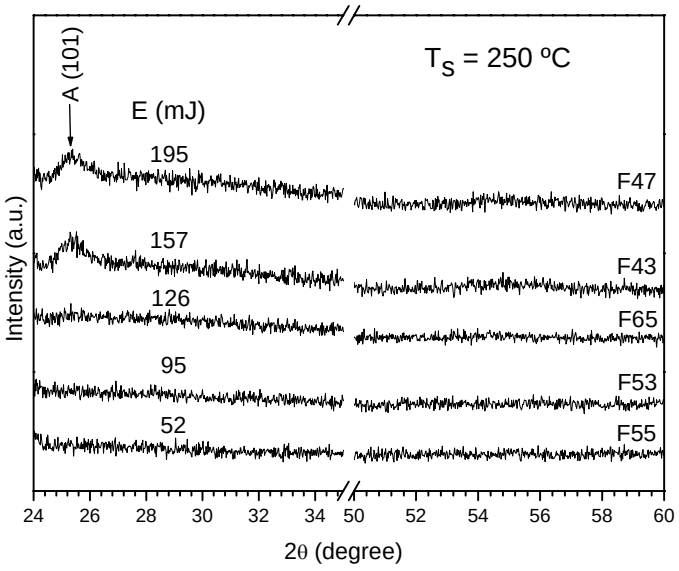

Figure 5.1 XRD patterns of Co-doped TiO_2 films grown on (0001) Al_2O_3 substrates in an Ar atmosphere, $P_T = 5.0\times10^{-1}$ mbar, at different laser energies, from 52 to 195 mJ at substrate temperature, T_S = 250 ºC.

We suppose that the absence of a diffraction peak is a consequence of the low laser output energy in the ablation process and not of insufficient thickness of the films; actually, sample F65 is thick enough (992 nm) to be able to provide a clear diffraction line. Low values of incident laser fluence generate particles arriving at the substrate surface with a reduced average kinetic energy. At T_S = 250 ºC, only a very small fraction of the ablated atoms have enough energy to migrate to the right positions and combine with other atoms at the film surface. That is why an amorphous structure was obtained for samples F55, F53 and F65. With the increasing of laser output energy to 157 mJ and further to 195 mJ, the anatase phase is formed – a low intensity and broad anatase peak, A(101), appears in samples F43 and F47 while no other phase was present.

The XRD patterns of the Co-doped TiO_2 thin films deposited at T_S = 310 ºC are shown in figure 5.2. The films are predominantly formed by a polycrystalline anatase phase, although a very small fraction of the rutile phase is also present. The XRD peak at about 25.388º is attributed to the (101) plane of anatase having an intensity of 100% according to the JCPDS database card nº. 21-1272. The second peak at 27.39º corresponds to the (110) plane of the rutile phase, with an intensity of 100% according to the JCPDS database card nº. 21-1276. The third peak is very broad and can be identified as due to a mixture of rutile and anatase. Rutile (211) plane diffracts at 54.41º, and anatase at 53.981º and 55.062º, corresponding to the (105) and (211) planes respectively. According to the JCPDS database cards mentioned above, for this third peak, rutile has an intensity of 60% and the two anatase peaks have an intensity of 20%.

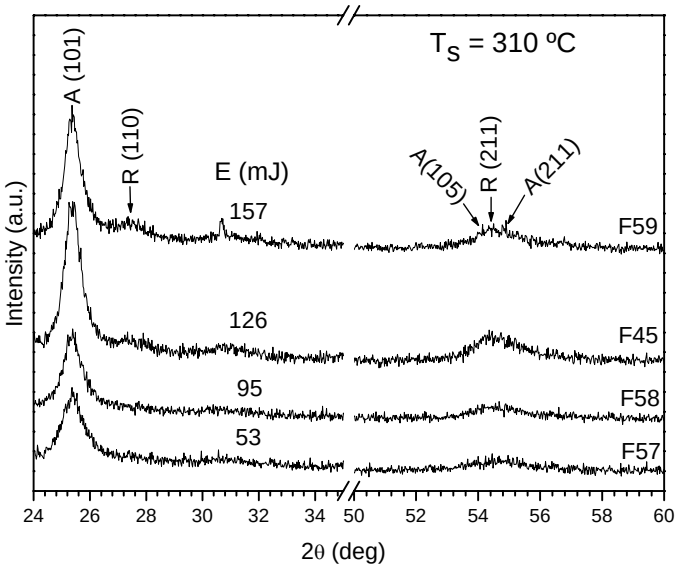

Figure 5.2 XRD patterns of Co-doped TiO_2 films grown on (0001) Al_2O_3 substrates in an Ar atmosphere, $P_T = 5.0\times10^{-1}$ mbar, at different laser energies, from 53 mJ to 157 mJ at substrate temperature, T_S = 310 ºC.

The Co-doped TiO_2 films prepared at high laser output energies for T_S = 250 ºC are weakly crystallized, while those prepared at higher substrate temperature, T_S = 310 ºC, display clear diffraction lines. This evolution can be explained by the increase of the atoms diffusion length (mobility) on the growing surface at higher substrate temperature, yielding a structural change from amorphous to polycrystalline material.[1] The crystallite size of the samples obtained at T_S = 310 ºC was estimated using Scherrer's equation (see eq. (4-5)). The average crystallite size increased from 9 ± 1.2 to 11.5 ± 1.2 nm *vs*. laser energy as can be seen in figure 5.3.

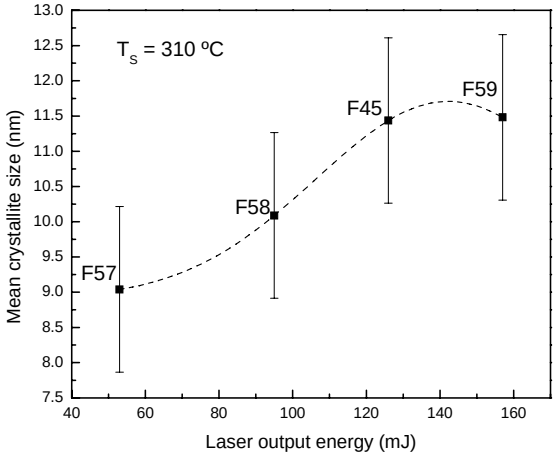

Figure 5.3 Mean crystallite size of Co-doped TiO_2 films deposited on (0001) Al_2O_3 substrates as a function of laser output energy. The curve drawn through the data points is for guidance only.

It is known that the deposition rate is smaller at the point situated in front of the focus position of the laser beam. This is due to the atoms arriving at the substrate with very high kinetic energy which will re-sputter the weak bonded atoms from the growing surface,

producing a decrease of the deposition rate/re-sputtering rate (D/R) ratio. This could explain the improving of the crystalline quality for samples F43 and F47 with increasing laser energy. So, a critical parameter for the quality of a deposited film is the kinetic energy of the particles impinging on the substrate. A similar influence of laser fluence upon the films quality can be noticed for those obtained at the highest substrate temperature. There is a clear difference between the films prepared at 53 and 95 mJ from those at higher fluences (126 and 157 mJ).

Besides film crystallinity, laser fluence also affects the deposition rate. The deposition rate probably corresponds to the nucleation density at the surface of the growing film since both depend on the amount of energetic species ablated from the target and arriving to the substrate through the deposition atmosphere.[2] Rising the laser fluence to 6.4 J/cm^2 and above led to an increase of the number of particles with kinetic energy high enough to attain the substrate surface, resulting in thicker films. In our experiments at 250 ºC, for instance, the deposition rate/pulse increased from 5 pm/pulse to 8.7 pm/pulse for a laser energy variation from 95 mJ to 195 mJ.

Optical properties

The optical properties – transmission, absorption, and optical bandgap of the Co-doped TiO_2 films were investigated as a function of laser output energy, for the two substrate temperature values given above .

Transmittance spectra in the UV-VIS-NIR range were recorded for Co-doped TiO_2 films prepared at different laser output energies and substrate temperature. The results are shown in figures 5.4 and 5.5. The observed oscillations, i.e. interference fringes, are due to multiple reflections in the layer.

Figure 5.4 presents the transmittance spectra of the as as-deposited films for laser output energy of 157 and 195 mJ (a), and 52 and 95 mJ (b), the films having been grown on (0001)Al_2O_2 substrate at 250 ºC. In Fig. 5.4 (c), the substrate temperature was increased up to 310 ºC and the laser energy varied between 52 mJ and 157 mJ.

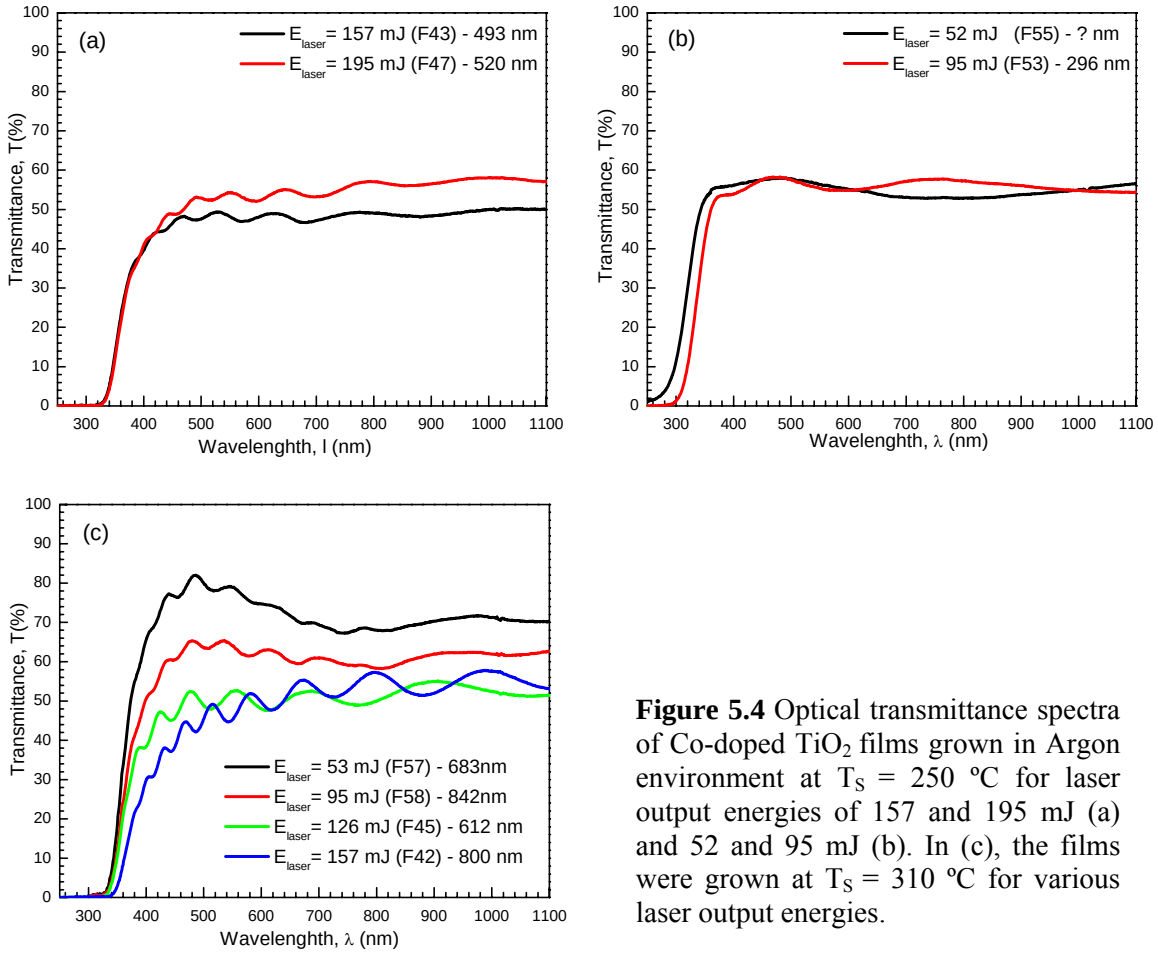

Figure 5.4 Optical transmittance spectra of Co-doped TiO_2 films grown in Argon environment at T_S = 250 ºC for laser output energies of 157 and 195 mJ (a) and 52 and 95 mJ (b). In (c), the films were grown at T_S = 310 ºC for various laser output energies.

The observed intensity oscillations in the 450 – 800 nm region of the spectra are due to optical interference effects whereas the features observed at < 400 nm are assigned to electronic band-gap transitions. The lack or reduced number of oscillations observed in the visible region of samples F55 and F53 (Fig. 5.4b) are an indication that these samples are quite thin. In general, films show a medium transparency with transmittance values falling in the range of 50% − 60 %. However, for the more crystalline films grown at 310 ºC there seems to be a correlation between the laser energy and transmittance through the effect of particle size. Indeed, as particle size (as determined by XRD) increases with laser energy, films become more opaque. This might be due to an increase of surface roughness associated with the increase of particle size which would promote the increase of light scattering by film's surface.

The influence of laser fluence on the optical band gap energy was investigated by using the transmittance curves and the procedure described in section 4.3.6. The results are plotted in

figure 5.5. An optical cut off at λ = 386 nm (corresponding to E_g^i = 3.2 eV) can be inferred for the films obtained by ablating with E_{laser} = 157 mJ and E_{laser} = 195 mJ, at T_S = 250 ºC. The observed absorption edges in the present work are consistent with the values reported in literature for the anatase TiO_2. We did not notice any appreciable change in the optical spectra for the sample obtained at E_{laser} = 95 mJ. As sample F55 presents very indistinct maxima and minima, the error in thickness determination is very high and it was not possible to determine the E_g^i value for this sample.

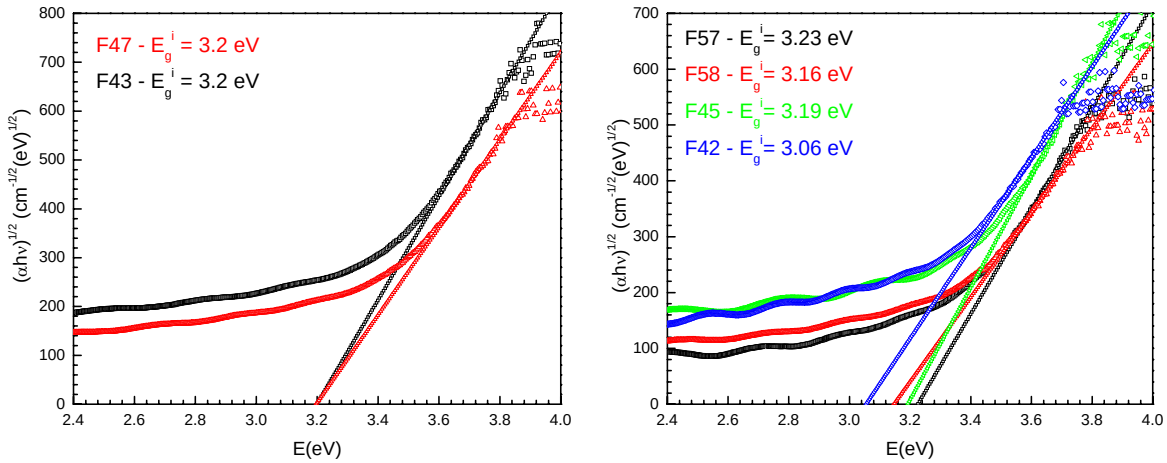

Figure 5.5 Photon energy dependence of SQRT(αhν) for Co-doped TiO_2 films, identified through their labels. Straight lines represent linear fits to the high energy region of the curves. Values for the band gap of the films are also shown in the figures. Left panel: T_S = 250 ºC; right panel: T_S = 310 ºC.

On the right side of the figure, we compare the optical data for the Co-doped TiO_2 films deposited at T_S = 310 ºC. The absorption edge shows a clear shift signifying the influence of incorporated Co on the electronic states. Such shifts have been found in diluted magnetic semiconductor systems. The E_g^i increases with increasing substrate temperature from 250 to 310 ºC for the lower laser energy value i.e. 53 mJ (E_g^i = 3.23 eV) but then, as films become more crystalline, the E_g^i decreases down to 3.06 eV (for the F42 film). Also the phase composition of these films can be responsible for the decrease of the band gap – though in very low concentration the rutile phase, which has a lower band gap energy than anatase is clearly present in sample F42, as revealed by the XRD pattern.

Rutherford Backscattering Spectrometry (RBS) data

Some of the Co-doped TiO_2 films were analysed by RBS in order to obtain another measurement of the thickness of the samples besides their chemical composition (stoichiometry). Samples were bombarded with both ^4He ions and protons. The depth profiles of the elements were extracted from the data using a simulation program (RUMP, developed by L.R. Doolittle[3]).

The recorded spectra are shown in figure 5.6.

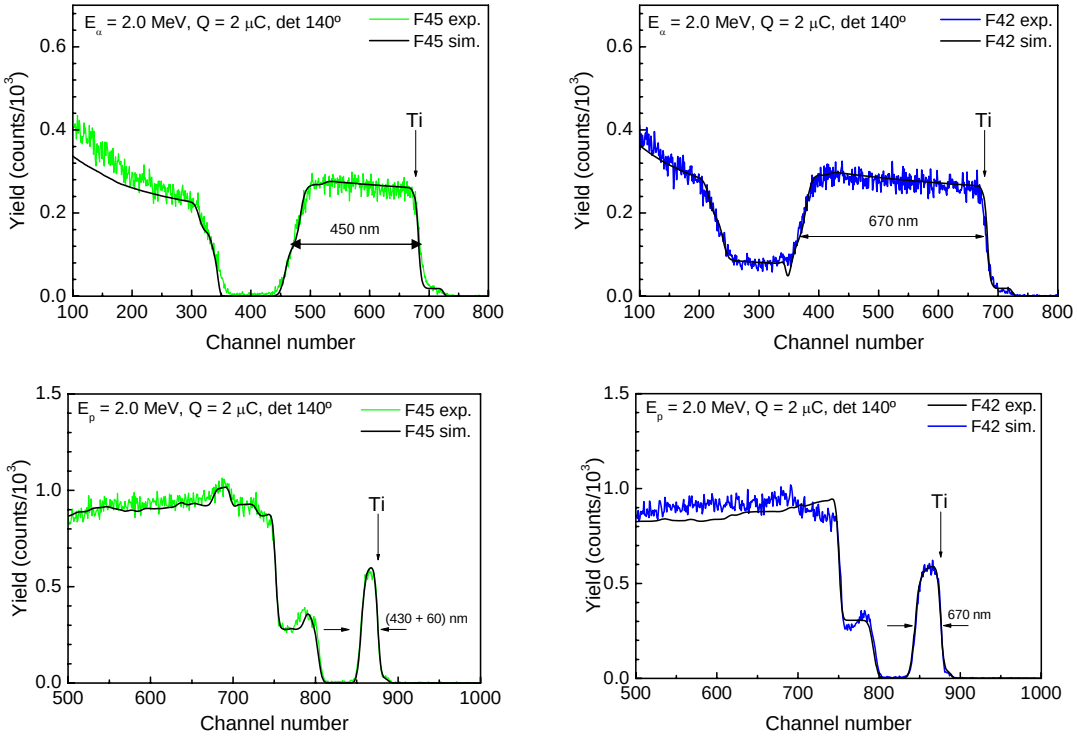

Figure 5.6 RBS spectra of Co-doped TiO_2 thin films deposited on (0001)Al_2O_3 substrate recorded for $^4He^+$ incident energy of 2 MeV (top) and $^1H^+$ incident energy of 2 MeV (bottom), and the corresponding theoretical simulations.

The RBS spectra and their fits indicate that the films are homogeneous along depth, as shown by the plateau in the Ti distribution profile, and that the diffusion of the Co is relatively uniform. The thickness of the films, *d*, was determined from the number (*Nd*) of atoms per unit area of the film (see eq. (4-7)) assuming that they consist only of anatase for which we can calculate the atomic density *N* as follows:

ρ (anatase) = 3.87 g/cm^3 = 2.92 × 10^{22} TiO_2/cm^3

$N = 3 \times \rho$ (anatase) = 8.75 × 10^{22} at./cm^3

The composition of the films show a slight oxygen excess of a few at.% while the Co concentration is approximately 1 at.%. Table 5.2 summarizes the results of the simulations.

Table 5.2 Film thickness and stoichiometry obtained from RUMP simulation

RBS analysis with α-particles	**Sample F45**	[O+Co]:[Ti] = 2.25:1 ⇔ $TiCo_{0.05}O_{2.20}$ ⇔ $\mathbf{Ti_{0.95}Co_{0.05}O_{2.1}}$ $(Nd) = 3750\times10^{15}$ /cm^2 ; $d \sim 430$ nm (using $\rho_{anatase}$) $(Nd)_{interface} = 500\times10^{15}$ /cm^2 ; $d \sim 60$ nm (using $\rho_{anatase}$)
	Sample F42	[O+Co]:[Ti] = 2.50:1 ⇔ $TiCo_{0.05}O_{2.45}$ ⇔ $\mathbf{Ti_{0.95}Co_{0.05}O_{2.4}}$ $(Nd) = 5700\times10^{15}$ /cm^2 ; $d \sim 650$ nm (using $\rho_{anatase}$) $(Nd)_{interface} = 500\times10^{15}$ /cm^2 ; $d \sim 60$ nm (using $\rho_{anatase}$)
RBS analysis with protons	**Sample F45**	[O+Co]:[Ti] = 2.13:1 ⇔ $TiCo_{0.03}O_{2.10}$ ⇔ $\mathbf{Ti_{0.97}Co_{0.03}O_{2.1}}$ $(Nd) = 3900\times10^{15}$ /cm^2 ; $d \sim 450$ nm (using $\rho_{anatase}$)
	Sample F42	[O+Co]:[Ti] = 2.13:1 ⇔ $TiCo_{0.03}O_{2.10}$ ⇔ $\mathbf{Ti_{0.97}Co_{0.03}O_{2.1}}$ $(Nd) = 5900\times10^{15}$ /cm^2 ; $d \sim 670$ nm (using $\rho_{anatase}$)

The best fit of the spectra recorded for $^4He^+$ ions were obtained by considering an interfacial layer, which is clearly observed on the spectra recorded with protons (peak at < 800 nm). It was not possible to identify the chemical composition of this layer, therefore its origin remains unknown.

In general, film thickness evaluated through RBS measurements is lower than that obtained from the optical absorption data. This can be due to an excessive density being used in the RBS calculation which might suggest that the films are not so dense as the bulk material.

5.3 Effect of ambient total pressure (II)

In order to investigate the effect of the working pressure on the growth process of the films we have conducted a set of depositions for argon pressures between 7.0×10^{-2} and 7.0×10^{-1} mbar, keeping the substrate temperature at 310 ºC and the laser output energy at 157 mJ. A second set of depositions was performed for a substrate temperature of 250 ºC and laser output energy of 195 mJ, using argon pressures between 2.5×10^{-1} mbar and 7.5×10^{-1} mbar. In both sets of experiments the argon flow rate was maintained at 30 sccm*. These experimental conditions are summarized on table 5.3.

Table 5.3 Growth parameters and film thickness

Sample	Laser output energy (mJ)	F (J/cm^2)	T_S (ºC)	P_T (mbar)	Φ_{Ar} (sccm)	No. of pulses	Thickness (nm)	Thickness /pulse (Å/pulse)
F86	157	6.4	310	7.0×10^{-2}	30	60 000	485	0.081
F84				1.0×10^{-1}		"	558	0.093
F83				2.0×10^{-1}		"	–	–
F63				3.0×10^{-1}		"	1249	0.208
F61				4.0×10^{-1}		"	1268	0.211
F42				5.0×10^{-1}		"	800	0.133
F60				6.0×10^{-1}		"	653	0.106
F62				7.0×10^{-1}		120 000	814	0.068
F52	195	7.9	250	2.5×10^{-1}		60 000	1604	0.267
F47				5.0×10^{-1}			725	0.121
F51				7.5×10^{-1}			359	0.060

Figure 5.7 displays the deposition rate/pulse as a function of the total pressure for the films described in the previous table. The decreasing tendency observed as the argon pressure increases can be explained by the increase of particles scattering due to collisions with the background gas. The similar values of the rate/pulse for the two deposition runs show that the temperature is not modifying the condensation rate between 250 ºC and 310 ºC. However, it is difficult to explain the low values obtained at the lowest pressures below 1.0×10^{-1} mbar which are around four times smaller than expected.

* ϕ (sccm) = $\phi \times 1.688 \times 10^{-2}$ mbar dm^3 s^{-1} $\Rightarrow$ 30 sccm = 0.5 mbar dm^3 s^{-1}

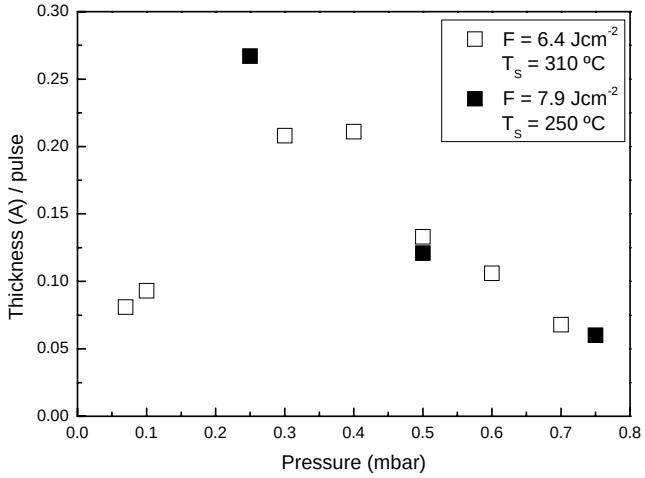

Figure 5.7 Film thickness deposited per laser pulse *vs.* Argon pressure

Possibly, these low values of the amount of ablated material at low argon pressure might be due to the fact that the angular distribution of the ejected material from the target is narrow as compared with the high pressure distribution; therefore, it might have happened that the substrate was not well positioned with regard to the ablation plume.

Crystal structure/phase composition

The XRD patterns of the thin films prepared under the conditions presented in table 5.3 are shown in figures 5.8 (E_{laser} = 157 mJ; T_S = 310 °C) and 5.9 (E_{laser} = 195 mJ; T_S = 250 °C). The films exhibit both anatase and rutile phases. While rutile is the dominant phase at low values of P_T, anatase is formed at the highest pressures; therefore, it is clear that the total pressure in the deposition chamber is a very important parameter that defines the crystallographic structure of the Co-doped TiO_2 films. In the range of growth conditions used in these experiments, both polycrystalline and amorphous structures were obtained. No matter the film thickness, an important XRD-signal always came from the (0001) Al_2O_3 substrate which was eliminated by cutting the spectra between 37-50 deg. Furthermore, neither a Co peak nor a cobalt oxide peak were detected in the spectra.

In the next paragraphs we will discuss in more detail the effect of argon pressure on the quality of the films through the analysis of the ablation plume.

Figure 5.8 shows the diffraction peaks indexed on the basis of the rutile and anatase phases (JPCDS filecards 21-1272 and 21-1276). One can see that the rutile phase is easily formed in low ambient argon pressures (7.0×10^{-2} − 2.0×10^{-1} mbar). The film prepared at P_T = 7.0×10^{-2} mbar is characterized by a narrow reflection peak of rutile, R(101). No other

reflection lines were detected. By increasing the total pressure from 7.0×10^{-2} mbar to 2.0×10^{-1} mbar the films with rutile structure display more reflexion lines, with the highest intensity coming from the (101) lattice plane. At a pressure of ~ 3.0×10^{-1} mbar starts the growth of the anatase phase, and between $3 - 4 \times10^{-1}$ mbar the diffraction peaks of anatase and rutile have similar intensities. At higher pressures the anatase phase is prevalent whereas a small rutile signal is always present.

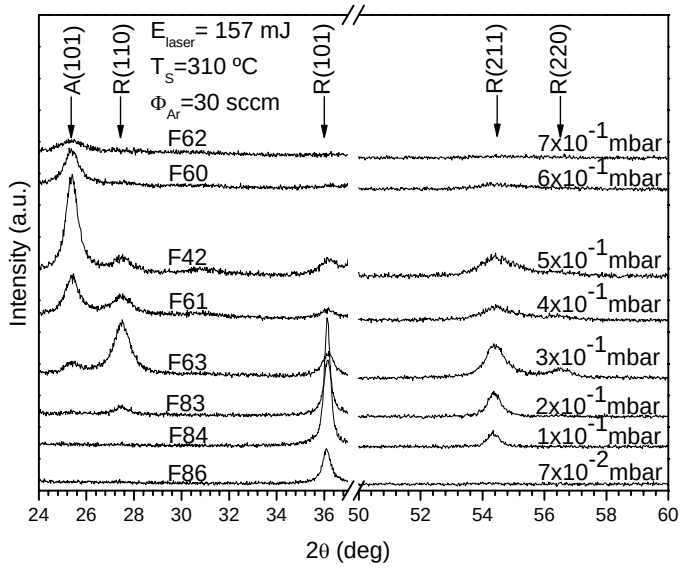

Figure 5.8 XRD θ-2θ scanning patterns of Co-doped TiO_2 thin films grown on (0001) Al_2O_3 substrates, at total pressures ranging from 7.0×10^{-1} mbar to 7.0×10^{-2} mbar. Φ_{Ar} = 30 sccm, T_S = 310 ºC, laser frequency = 20 Hz, and F = 6.4 J/cm^2.

As can be seen in figures 5.8 and 5.9, increasing the total pressure produces a loss of crystallinity and the disappearance of the rutile phase. A similar dependence on pressure has been reported previously for the PLD growth of rutile at 700 ºC.[4]

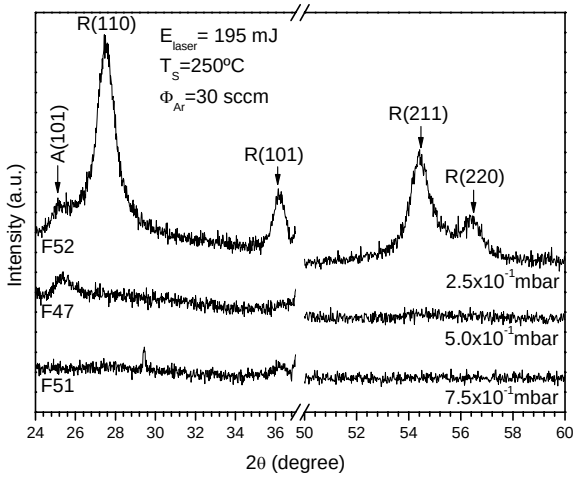

Figure 5.9 XRD θ-2θ scanning patterns of Co-doped TiO_2 thin films grown on (0001) Al_2O_3 substrates, at total pressures ranging from 2.5×10^{-1} mbar to 7.5×10^{-1} mbar. Φ_{Ar} = 30 sccm, T_S = 250 ºC, laser frequency = 20 Hz, and F = 7.9 J/cm^2.

Thus, the total pressure has a strong effect on the crystallinity and phase composition

(anatase *vs.* rutile) of the Co-doped TiO_2 thin films prepared by PLD. The effect of total pressure can be discussed in terms of the roles played by *i)* the plume confinement and *ii)* the chemical role.

When penetrating a background gas, the plasma plume producing the film growth is divided into distinct "fast" and "slow" velocity distributions where the fast component is target material that has penetrated the background gas without undergoing collisions, while the slow component is material that has undergone momentum-changing collisions with the background gas, or with other plume atoms. Therefore, in addition to giving rise to a shock wave, scattering by an inert background gas modifies both the shape and the velocity of an ablation plume. Furthermore, background gas ionisation induced by charge transfer collisions with fast ions in the ablation plume also plays an important role upon the structure, morphology and physical properties of the growing films.

In the case of film growth in a low argon gas pressure, the interactions between the ablated species and the background gas are weak. Energetic particles due to long mean free path land on the substrate and surface migration is enhanced *i.e.*, the kinetic energy of the source particles (particles ablated from the target) is sufficiently high to provide the surface mobility required to form a crystalline thin film.[5] An increase in the total pressure limits the mean free path and leads to a confinement of the vapour; the kinetic energy of the ablated species is reduced during the collisions with argon atoms. In the extreme case of ablation taking place in a very high pressure ambient gas, the loss of kinetic energy may lead to particles stucking together and depositing as aggregates on the substrate surface.

Okimura *et al.*[6] prepared TiO_2 films by rf magnetron sputtering using a mixture of Ar and O_2 gases and reported that the rutile phase is formed by the reaction of Ti^+ with O_2^-; the concentration of O_2^- is much higher at lower total pressure when high-energy electrons produce O_2^- ions via inelastic collisions. They showed that the energetic species impinging on the growing film are responsible for the formation of the rutile phase even if the substrate is at room temperature. Shibata *et al.*[7] studied the effect of a heating probe in reactive magnetron sputtering and reported that the anatase phase is the result of the reaction between neutral Ti and neutral O_2 or O_2^-, while the rutile phase results from the reaction between Ti^+ or activated Ti and O_2^-. Moreover, rutile is the high-temperature phase of TiO_2 in the equilibrium state, i.e. it has a higher activation energy of formation than anatase.

In addition to the fact that the activation energy of rutile is higher than that of anatase, at high total pressure (7.0×10^{-1} mbar) the anatase phase is formed because of the amount of oxygen present during the ablation process. The same argon flow (30 sccm) and low total pressure (7.0×10^{-2} mbar) result in less amount of oxygen in the chamber. The same argon flow (30 sccm) and high total pressure (7.0×10^{-1} mbar) result in a high amount of oxygen in the chamber. This effect will be studied in more detail in section 5.4.

In the pressure range from 7.0×10^{-2} to 2.0×10^{-1} mbar corresponding to the rutile formation, the peaks intensities (Fig. 5.8) do not correspond to those of XRD powder diagram. The R(101) peak intensity is strongly enhanced as compared to the others, especially for the sample produced at 1.0×10^{-1} mbar. The transition from rutile to anatase phase takes place between 3.0×10^{-1} and 4.0×10^{-1} mbar. Sample F63 presents a small (101) anatase peak and contains about 86% rutile and 14% anatase.[8] Sample F61, prepared at a higher pressure, displays an important component of anatase phase ~ 62% and a corresponding reduced rutile phase content of ~ 38%. As the pressure increases more (5.0×10^{-1} mbar) the anatase phase becomes prevalent (86%) and the rutile reduces to a small amount (14%). Further increment (6.0×10^{-1} mbar and 7.0×10^{-1} mbar) produces the disappearance of the rutile phase as well as the loss of film crystallinity mentioned previously. This can be explained by the oxygen incorporation into the film. Oxygen is one of the constituents of the TiO_2 compound being essential for the formation of the TiO_2 structure. It is known that when TiO_2 is heated under low pressure of O_2, TiO_2 loses oxygen from the lattice becoming an n-type semiconductor.[9]

In case of the films displayed in Fig. 5.9, the XRD spectra show the diffraction peaks of the Co-doped TiO_2 as follows: A(101), R(110), R(101), R(211) and R(220). The intensities of rutile phase peaks for sample F52 are similar with those of the TiO_2 powder diagram (R(110) - 100%, R(101) - 50%, R(211) - 60% and R(220) - 20%). No peak of any impurity phase appeared in the XRD patterns.

The crystallites' size can be estimated from the width of the Bragg reflection peaks using the Scherrer formula (eq. 4-5). Figure 5.10 displays the FWHM values (correlated with the crystallite dimension) *vs*. argon deposition pressure for the films shown in Fig. 5.8. The values of FWHM were estimated for the (101) lines either of anatase (samples F62, F60, F42, F61) or rutile (F63, F83, F84, F86). As a general tendency the FWHM ($\theta - 2\theta$ scan)

values increase for both phases as the total pressure increases. This means that the crystallite size decreases and results in films of poorer crystallinity. Thus, we can say that the crystallinity of the titanium dioxide films is optimal at 1.0×10^{-1} mbar for the rutile phase and at 5.0×10^{-1} mbar for anatase phase.

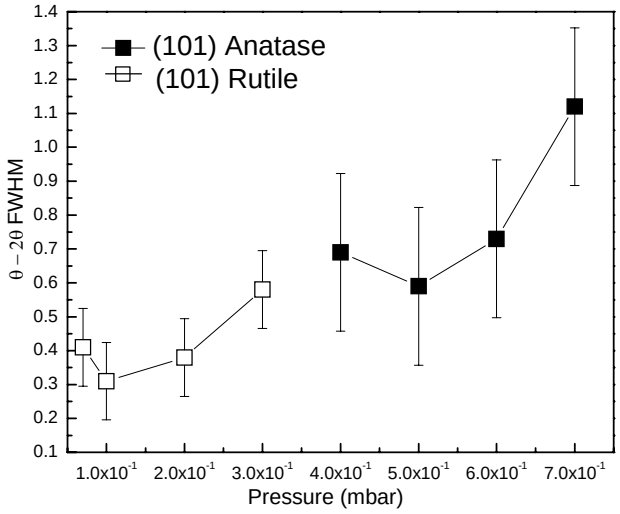

Figure 5.10 FWHM (θ−2θ scan) of the Bragg reflection peak *vs.* total pressure.

Optical properties

Here we present results illustrating how the optical properties of the films depend on the main deposition parameters. Measurements of light transmission were performed in the range from 300 to 1100 nm with a commercial spectrophotometer (see Chapter 4, section 4.3.6).

- ***"Low" laser energy (E_{laser} = 157mJ) and "high" substrate temperature (T_S = 310°C)***

Figure 5.11-a) displays the transmittance spectra of the Co-doped TiO_2 films as-deposited at different total pressure from 1.0×10^{-1} mbar to 7.0×10^{-1} mbar. The fringes noticed in the transmittance spectra are due to the interference phenomena in the thin films.

It is seen that the transmittance of the films decreases as the total pressure decreases. In other words the films deposited at low total pressure are more absorbing. This might be due to insufficient oxygen incorporation in the film during deposition. Another possible explanation could be the increase of surface scattering related to surface roughness due to increased film crystallinity.

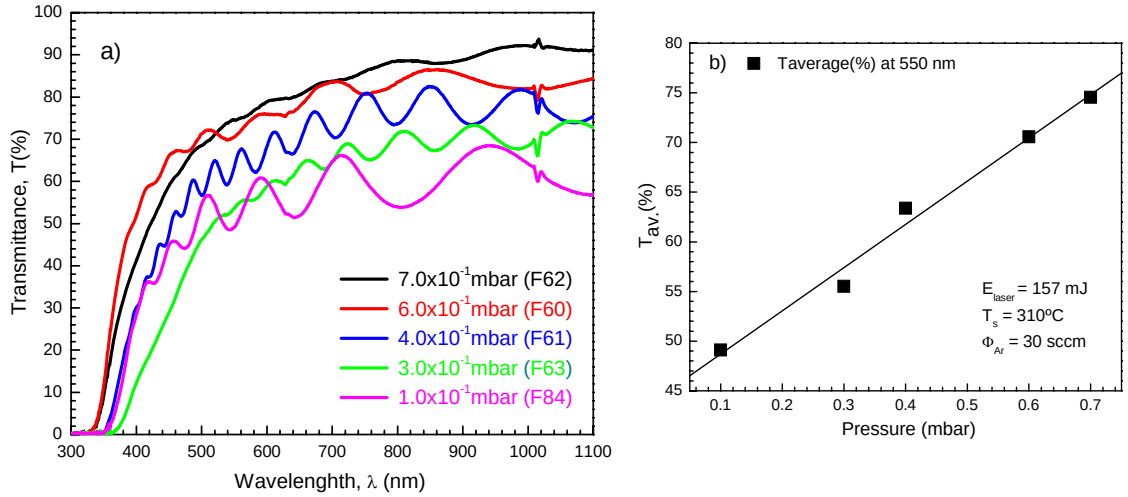

Figure 5.11 Optical transmittance spectra (a) and average transmission, $T_{av.}$, *vs.* Pressure (b) for Co-doped TiO_2 films grown in Ar environment at various total pressures, E_{laser} = 157 mJ and T_S = 310 ºC

Figure 5.11-b) shows the average transmission, $T_{av.}$, for visible light (integral value at 550 nm) calculated from the spectra in Fig. 5.11-a). No significant effect of film thickness was observed in the optical transmission of the films. The latter result as well as the average transmission values encountered in the pulsed laser deposited Co-doped TiO_2 films (between 49 - 75%) are in agreement with recent observations by other groups.

The thickness of the films, *d*, was calculated in the range 654 nm to 1268 nm from the optical transmission measurements, T(%), using equation (4-16). Assuming that intensity losses due to reflection may be neglected, the optical absorption coefficient, α, was calculated using equation (4-17). Figure 5.12 shows a Tauc plot of $(\alpha h\nu)^{1/2}$ versus hν.

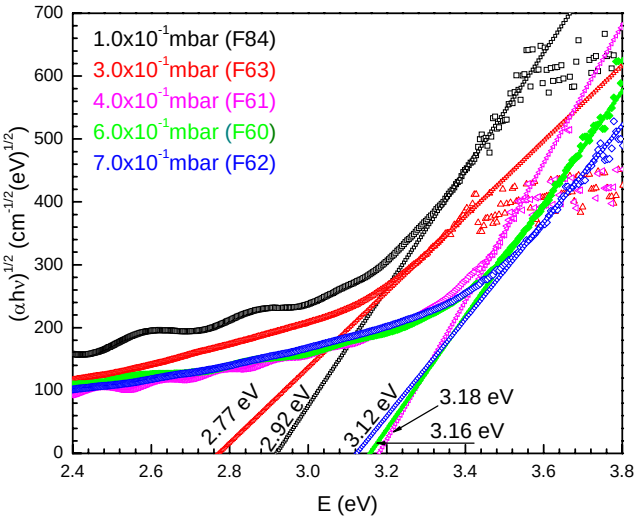

Figure 5.12 Photon energy dependence of the SQRT(αhν) for the Co-doped TiO_2 films deposited under the conditions described in Table 5.3. Straight lines represent linear fits to the high energy region of the curves. Values for the band gap of the films are also shown in the figure.

The high energy part of the curves was fitted by straight lines which were extrapolated to zero absorption giving the indirect band gap energies, E_g^i.

Table 5.4 Indirect band gap energy of the films grown at 310 ºC in argon atmosphere

Sample	P_T (mbar)	Phase composition	Crystallinity	E_g^i (eV)
F84	1.0×10^{-1}	100% rutile	+	2.92
F63	3.0×10^{-1}	86% rutile + 14% anatase	−	2.77
F61	4.0×10^{-1}	38% rutile + 62% anatase	+	3.18
F60	6.0×10^{-1}	100% anatase	−	3.16
F62	7.0×10^{-1}	100% anatase (amorphous)	− −	3.12

If the E_g^i values are compared with those for pure TiO_2 anatase (3.2 eV) and rutile (3.05 eV), it can be concluded that the optical band gap shifts to the red in the Co-doped films. This can be explained by the fact that the atomic potentials for Co are larger than those for Ti, the Ti-Co band would be lower than the pure Ti band in TiO_2 resulting in the red shift of the band edge, contrary to the results obtained by J.R. Simpson *et al.*[10] in their study.

On the other hand, the comparison of samples F62, F60 and F61, and of samples F63 and F84, show that as the pressure decreases the optical band gap increases (shifts to the UV) in the Co-doped films due to the transition from less crystalline material (even amorphous at 7.0×10^{-1} mbar) to a more crystalline thin film material.

- ***"High" laser energy (E_{laser}=195mJ) and "low" substrate temperature (T_S=250°C)***

The transmission spectra and average transmission, $T_{av.}$, for visible light (integral value at 550 nm) of the three Co-doped TiO_2 samples grown at "high" laser energy of 195 mJ and T_S = 250°C are shown in Fig. 5.13.

From the transmission curves it is likely that there is a correlation between the film thickness and the average transmission which decreases for thicker films. Sample F52 with a thickness of 1604 nm shows a $T_{av.}$ = 50% while for sample F51, 359 nm thick, $T_{av.}$ = 74%.

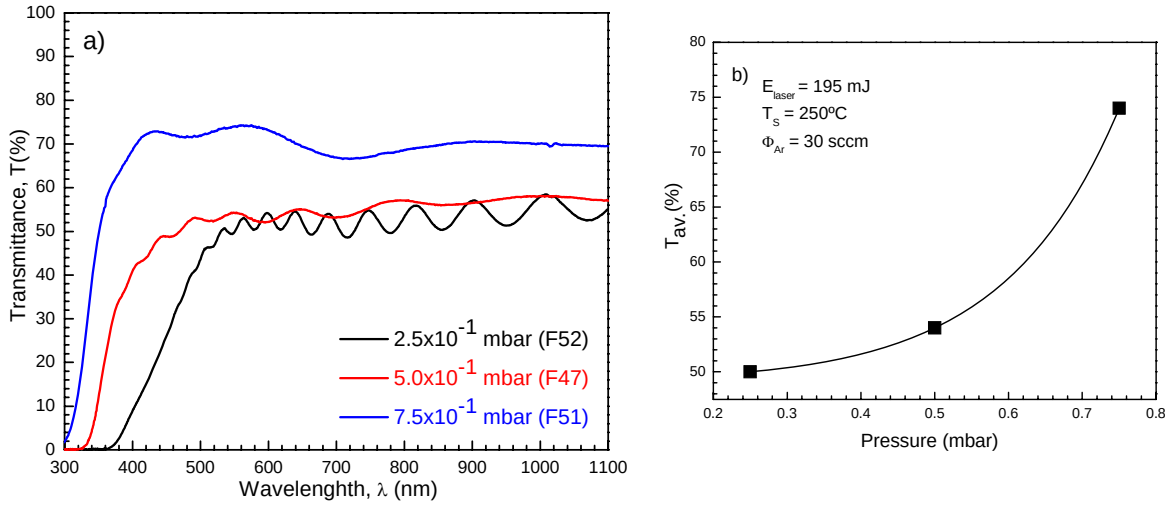

Figure 5.13 Optical transmittance spectra (a) and average transmission, $T_{av.}$, *vs.* pressure (b) for Co-doped TiO_2 films grown in Ar environment at various total pressures, E_{laser} = 195 mJ and T_S = 250 ºC.

In table 5.5, the indirect band-gap E_g^i values, estimated from the $(\alpha h\nu)^{1/2}$ *versus* photon energy plots, as indicated above, are shown together with pressure preparation conditions and crystallinity of the samples.

Table 5.5 Estimated energy gap, E_g^i, for films deposited at substrate temperature of 250 ºC in argon background gas.

Sample	P_T (mbar)	Phase composition / crystallinity	E_g^i (eV)
F52	2.5×10^{-1}	mainly rutile	2.77
F47	5.0×10^{-1}	mainly anatase	3.20
F51	7.5×10^{-1}	amorphous	3.29

The same trend with pressure as that observed for the films grown at higher temperature and lower fluence is also seen in the present case. Furthermore, the band-gap values obtained for the Co-doped TiO_2 films are in reasonable agreement with results from others. Wan Kyu Park *et al.*[11] reported on E_g = 3.25 ± 0.5 eV for $Ti_{1-x}Co_xO_2$ single phase rutile structure obtained by reactive co-sputtering for a substrate temperature in the range 250-450 ºC. Fa-Min Liu *et al.*[12] have reported on a red shift of the optical absorption edge with increasing substrate temperature (between 300 ºC and 400 ºC) for the Co-doped TiO_2 sandwich composite films deposited by alternatively using radio frequency reactive and direct current magnetron sputtering onto glass and silicon substrates. They have interpreted

the band gap decrease of their Co-doped TiO_2 films as the result of the diffusion of Co atoms into the TiO_2 matrix, which they attributed to the rising of the substrate temperature.

Chemical analysis by RBS

RBS spectra recorded over the samples of this series of experiments using either protons or α particles, and their fits, indicate that the films are homogeneous along depth and that the diffusion of the Co is relatively uniform. The composition of various films are given in table 5.6 and the RBS spectra shown on figures 5.14 and 5.15.

Table 5.6 Parameters obtained from RUMP simulation

RBS analysis with protons	**Sample F63** [O+Co]:[Ti] = 2.13:1 ⇔ $TiCo_{0.03}O_{2.10}$ ⇔ $\mathbf{Ti_{0.97}Co_{0.03}O_{2.1}}$ $(Nd) = 11300\times10^{15}$ /cm^2 ; $d \sim 1300$ nm (using $\rho_{anatase}$)
	Sample F52 [O+Co]:[Ti] = 2.13:1 ⇔ $TiCo_{0.03}O_{2.10}$ ⇔ $\mathbf{Ti_{0.97}Co_{0.03}O_{2.1}}$ $(Nd) = 12900\times10^{15}$ /cm^2 ; $d \sim 1470$ nm (using $\rho_{anatase}$)
RBS analysis with α-particles	**Sample F84** [O+Co]:[Ti] = 2.13:1 ⇔ $TiCo_{0.03}O_{2.10}$ ⇔ $\mathbf{Ti_{0.97}Co_{0.03}O_{2.1}}$ $(Nd) = 4400\times10^{15}$ /cm^2 ; $d \sim 500$ nm (using $\rho_{anatase}$) $(Nd)_{interface} = 400\times10^{15}$ /cm^2 ; $d \sim 40$ nm (using $\rho_{anatase}$)

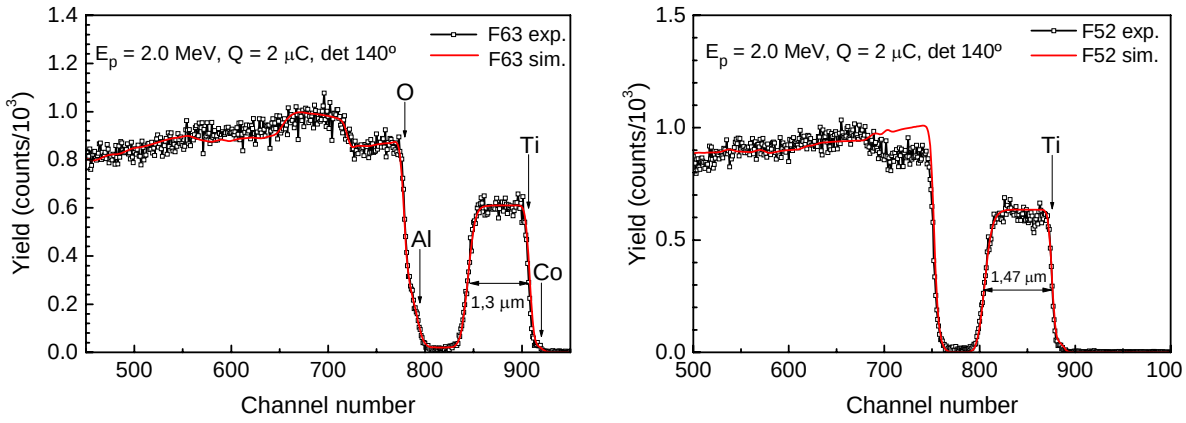

Figure 5.14 RBS spectra of samples F63 (left) and F52 (right) deposited on (0001)Al_2O_3 substrate and the corresponding theoretical simulations. The spectra were recorded with $^1H^+$ incident energy of 2 MeV.

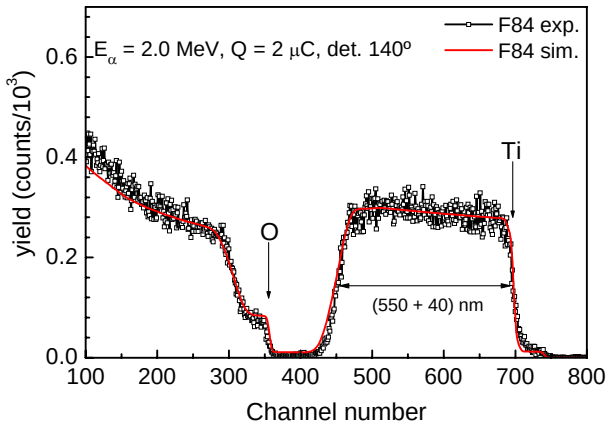

Figure 5.15 RBS spectra of sample F84 deposited on (0001)Al_2O_3 substrate recorded for $^4He^+$ incident energy of 2 MeV and the corresponding theoretical simulation

5.4 Effect of substrate temperature (III)

Two energy sources are important during PLD film growth, i.e. the kinetic energy of the arriving particles and the substrate temperature, both influencing the crystallographic structure and film morphology. The substrate temperature determines the crystallographic orientation when the kinetic energy is kept constant (e.g. by maintaining the distance between the target and the substrate, the laser fluence and the total pressure in the deposition chamber). An increase of the temperature enhances the surface mobility of the atoms and clusters arriving at the substrate surface. At higher growth temperature, the number of defects are minimized (due to surface mobility) and the film grows with the orientation of the substrate. The transition from random orientation to epitaxial film growth is observed at high temperature when the target-substrate distance is increased, leading to arriving species with lower kinetic energies. The variation of these two parameters − distance and temperature, give the unique opportunity to prepare films with crystallographic features that vary from amorphous to epitaxial without changing the pressure of the background gas or the type of substrate.

In order to study the effect of the substrate temperature on the structural and optical properties of the samples, several Co-doped TiO_2 thin films were deposited onto heated substrates by pulsed laser ablation at laser fluence of 6.4 Jcm^{-2}. The background gas consisted on pure argon (Φ_{Ar} = 30 sccm), and the working pressure was 5.0×10^{-1} mbar. The films were grown onto heated substrates in the range from 200 ºC to 350 ºC. The deposition time was the same for all the samples corresponding to 60 000 pulses, and the samples' thickness was measured in the range of 500 - 800 nm.

Table 5.7 PLD thin films deposition parameters.

Sample	Laser output energy (mJ)	F (J/cm^2)	T_S (ºC)	P_T (mbar)	Φ_{Ar} (sccm)	No. of pulses	Thickness (nm)
F44	157	6.4	200	5.0×10^{-1}	30	60 000	570
F43			250				493
F42			310				800
F56			350				565

Some of the samples were analysed by RBS using a beam of α particles and/or protons in order to determine the stoichiometry of the grown material. The same procedure as in previous sections was followed and the results are summarised here below.

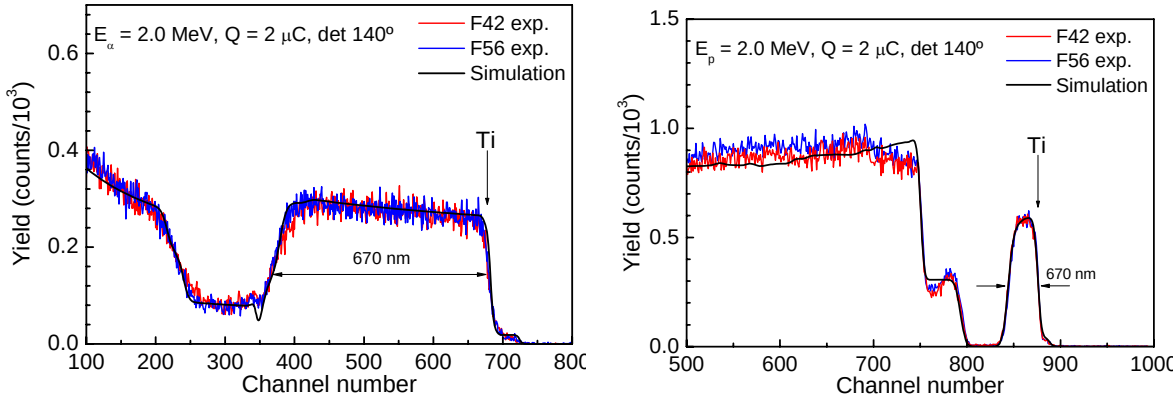

Figure 5.16 RBS spectra of samples F42 and F56 deposited on (0001)Al_2O_3 substrate. Left panel spectrum was recorded for $^4He^+$ incident energy of 2 MeV while on the right panel $^1H^+$ incident energy of 2 MeV was used. The RUMP simulations are also plotted.

If the RBS spectra of samples F42 and F56 are compared, it can be seen that the samples should have the same composition; the spectra of these samples overlapp i.e., if the structures are identical the spectra have equal heights pointing out the same value for film composition. Like for the samples in section 5.2. a slight oxygen excess (3%) was determined; the Co concentration is approximately 1 at.%, both values relating to $TiO_{2.1}$+Co_x.

The simulation of the spectra recorded with α's and protons with the RUMP code yield the same results for both samples, F42 and F56; those of F42 were already displayed on table 5.2.

Crystalographic structure

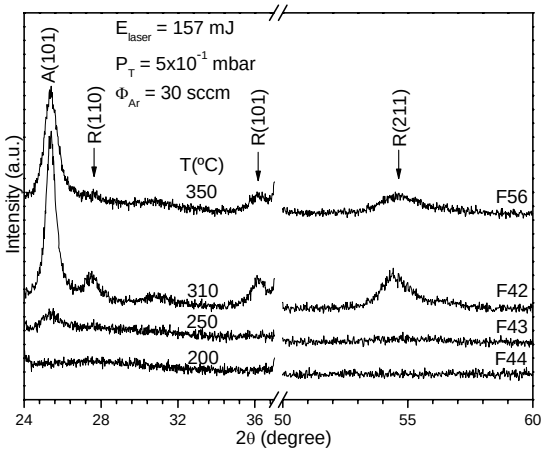

Figure 5.17 XRD patterns of Co-doped TiO_2 films grown on (0001) Al_2O_3 substrates in an Ar atmosphere, $P_T = 5.0\times10^{-1}$ mbar, at different substrate temperatures.

The Co-doped TiO_2 thin films deposited in argon environment at 200 ºC exhibit diffractograms showing their amorphous behaviour, while the film grown at 250 ºC already points out for a certain degree of crystallisation − just one diffraction line, the A(101), may be observed although quite broad with very low intensity. Increasing the substrate temperature to 310 ºC, we get a mixture of anatase (86.2%) and rutile phases (13.8%). All the positions of the observed diffraction peaks have been obtained in good agreement with the JCPDS file cards 21-1272 for anatase and 21-1276 for rutile and, therefore, the crystallites are randomly oriented in these films. For a substrate temperature of 350 ºC the sample becomes again less crystalline. Both the observed diffraction peak positions and relative intensity ratios are maintained.

Recently, S. Amoruso *et al.*[13] have demonstrated the influence of the substrate temperature on the internal energy of the ablated species; therefore, T_S has a double effect acting on the surface mobility in a direct way and also via its coupling with particles' energy.

Optical properties

Next we discuss the influence of the growth temperature on the optical properties of the Co-doped TiO_2 films. As can be seen in Fig. 5.18, the transmittance is lowered as the substrate temperature increases during film growth.

In general, the absorption (transmittance) of TiO_2 films increases (decreases) with the increase of the substrate temperature, the variation being smaller for thicker films. The decrease of transmittance in these films may be a result of the insufficient incorporation of

oxygen in the films during deposition since the condensation of oxygen decreases at elevated substrate temperature, as observed by Ritter[14] and others. Kuster and Ebert[15] also observed an increase of the absorption of TiO_2 films with increasing substrate temperature, and have explained this increase on the basis of decomposition of TiO_2 at elevated temperatures.

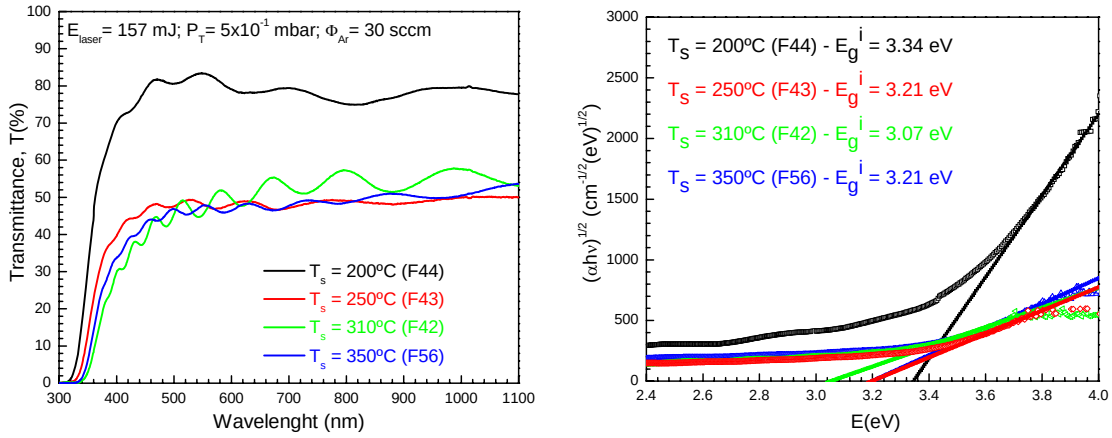

Figure 5.18 Optical transmittance spectra a) and Tauc plot b) for the Co-doped TiO_2 films displayed in Fig. 5.17.

On the other hand, the lower transmittance of the films deposited above 250 ºC can also be correlated with the crystallinity of the samples which induces a rougher surface leading to enhanced light scattering.

5.5 Effect of Argon flux (IV)

The interaction of laser ablation plumes with a background gas has been receiving increased attention due to its importance in pulsed laser deposition[16], nanoparticles formation and growth[17-19], and laser micromachining.[20] Compared with expansion into vacuum, the interaction of the plume with an ambient gas is a far more complex dynamic process due to the appearance of new physical processes such as deceleration, thermalization of the ablated species, interpenetration, recombination, formation of shockwaves and clustering.[21-26] Scattering by a background inert gas modifies both the shape and the velocity of an ablation plume, besides the development of a shock wave.[27,28] Here we study the effect of introducing an inert gas (argon) at different flow rates on the structural, morphological and optical properties of Co-doped TiO_2 films.

The thin films were grown onto Al_2O_3(0001) substrates (*c-cut* sapphire) at a fixed substrate temperature of 310 ºC and laser output energy of 126 mJ for two values of total pressure, $P_T = 5.0\times10^{-1}$ mbar and $P_T = 7.0\times10^{-2}$ mbar. Only the argon flow rates, Φ_{Ar}, were modified while the total pressure was kept constant. The deposition conditions are summarized in table 5.8.

Table 5.8 PLD thin film growth parameters

Sample	Laser output energy (mJ)	F (J/cm^2)	T_S (ºC)	P_T (mbar)	Φ_{Ar} (sccm)	No. of pulses
F78	126	5.1	310	5.0×10^{-1}	6	60 000
F45					30	
F74					180	
F85					270	
F82				7.0×10^{-2}	6	
F81					30	

Crystalline structure

The XRD patterns of the films prepared at a total pressure of 5.0×10^{-1} mbar are shown in Fig. 5.19. The F78 sample prepared at a low argon flow of 6 sccm displays mainly the anatase (101) diffraction peak; raising the argon flow to 30 sccm results in improving the crystallinity of the anatase phase (sample F45, crystallite size = 11.4 nm), and further increase of the argon flux leads to the development of the rutile phase as indicated by the presence of the (110), (101) and (211) rutile diffraction peaks.

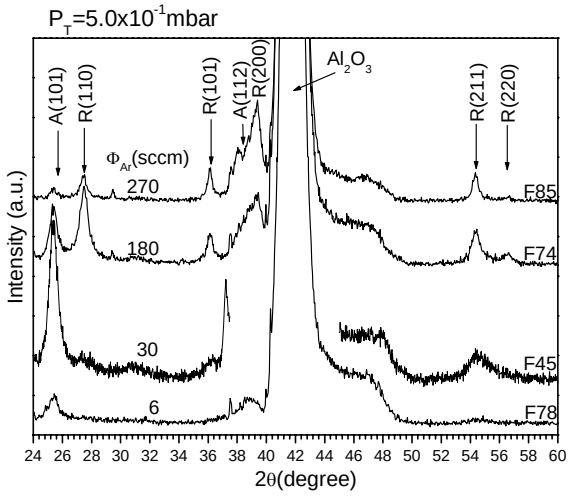

Figure 5.19 XRD θ-2θ scanning patterns of Co-doped TiO_2 thin films grown on (0001) Al_2O_3 substrates, at argon fluxes, Φ_{Ar}, ranging from 6 to 270 sccm. The substrate temperature, pulse repetition rate and laser fluence were kept constant at 310 ºC, 20 Hz and 5.1 J/cm^2, respectively. Total pressure is 5.0×10^{-1} mbar.

The appearance of the rutile phase is due to the decrease of the oxygen partial pressure in the chamber, which favours rutile phase formation, as demonstrated by the two additional samples, F74 and F85.

A large amount of material is evaporated during the very short time of laser pulse. The oxygen originates exclusively from the oxide target. We have seen in section 5.2 that the chemical composition of sample F45 as determined by Rutherford Backscattering Spectroscopy (with protons) could be written as $Ti_{0.97}Co_{0.03}O_{2.10}$; equivalent measurements performed on samples F74 and F85 gave a similar stoichiometry. Therefore, RBS measurements lead one to conclude that the amount of oxygen provided by the target during the ablation process is much larger than that required for growing Co-doped TiO_2 films. However, only a fraction of the oxygen is released as atomic oxygen (neutrals and ions), while the remaining part is ejected as molecular oxygen. Due to inefficient adsorption at the surface, the adsorption probability of O_2 is less than unity, much lower than for atomic oxygen. The fact that the oxygen molecules have a lower probability of remaining at the surface makes it necessary, in general, to use an additional source of oxygen for the effective oxidation of the cations during film growth. But as mentioned previously in section 4.1.6 , the target contains a surplus of oxygen and since the aim of our study was to produce oxygen-deficient films, argon was used to lower the oxygen partial pressure to further reduce the quantity of oxygen absorbed by the sample.

Keeping the total pressure inside the chamber at a constant value while incrementing the argon flow rate requires a system with higher vacuum extraction capacity. If the amount of oxygen liberated remains at a constant value while the system's vacuum extraction capacity is increased, the oxygen partial pressure starts to decrease and the growth of the rutile phase is preferred. Consequently, the increase of argon flux to 180 sccm and 270 sccm resulted in phase transition from anatase to rutile in sample F74 and in a predominantly rutile phase and amorphisation of the anatase phase in sample F85. A high oxygen partial pressure will, in turn, lead to an excess of oxygen in the films, allowing formation of the anatase phase as a result of its lower density compared to the rutile phase.

The analysis of the most intense peaks of the XRD spectra − for which the JCPDS database cards no. 21-1272 and 21-1276 specify an intensity of 100% for the anatase phase (101) lattice plane and the rutile phase (110) lattice plane respectively, clearly indicates that the film phase composition and structure depends on the magnitude

of the argon flow. The data demonstrating this dependence are given in Table 5.9 and illustrated in figure 5.20. There is a gradual transition from an anatase-dominated to a rutile-dominated composition with increasing argon flow.

Table 5.9 Percentage of the anatase phase (W_A) and rutile phase (W_R) of the studied Co-doped TiO_2 thin films obtained at a total pressure $P_T = 5.0\times10^{-1}$ mbar.

Sample	Φ_{Ar} (sccm)	W_A (%)	W_R (%)
F78	6	100	-
F45	30	92	8
F74	180	47	53
F85	270	25	75

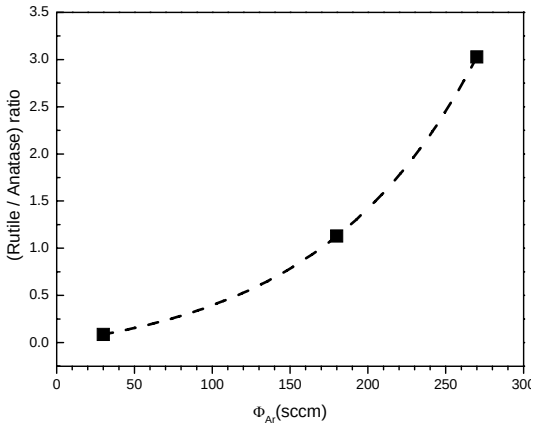

Figure 5.20 Argon flux favours the rutile phase growth relative to that of anatase phase. The dashed line is for visual guidance only.

The transition from mixed orientation to highly oriented film growth is now observed with the reduction of the total pressure and, consequently, of the oxygen partial pressure. Attenuation of the total pressure to 7.0×10^{-2} mbar, and control of the argon flow, allow the preparation of films with high crystallographic orientation without changing other parameters or even the substrate.

These results confirm the prediction of rutile phase formation at low oxygen partial pressure, an effect that has previously been observed for samples obtained with comparable experimental parameters but at a total pressure of 5.0×10^{-1} mbar and high argon flow rates. If we compare sample pairs F78/F82 and F45/F81, it can be seen that application of the same argon flow rate, but at two different total pressure values, leads to the formation of two completely different phases: anatase at a total pressure of 5×10^{-1} mbar and highly oriented rutile phase at 7.0×10^{-2} mbar. The XRD patterns of the Co-doped TiO_2 thin films deposited at $P_T = 7.0\times10^{-2}$ mbar are shown in Fig. 5.21. The films are rutile phase without any impurity phase.

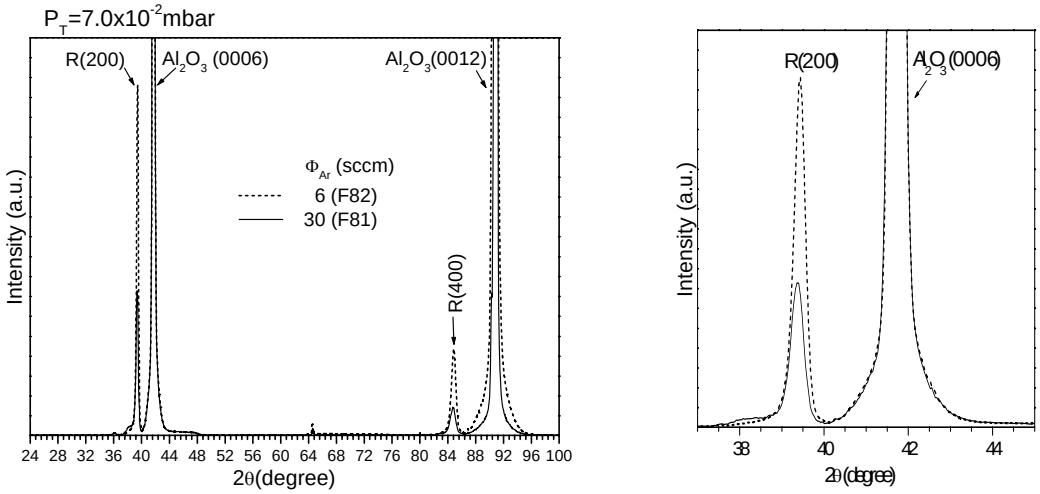

Figure 5.21 XRD θ-2θ scanning patterns of Co-doped TiO_2 thin films grown on (0001) Al_2O_3 substrates, at argon fluxes, Φ_{Ar} = 6 and 270 sccm. The substrate temperature, pulse repetition rate and laser fluence were kept constant at 310 ºC, 20 Hz and 5.1 J/cm^2, respectively. Total pressure is 7.0×10^{-2} mbar. Right panel: magnification of the 2θ range: 38−44º.

Both films deposited on Al_2O_3(001) show only the (200) and the (400) reflections, indicating that the films are highly oriented to the substrate. The XRD peak at about 2θ = 39.45º is attributed to the (200) plane of the rutile phase with an intensity of 8% according to the JCPDS database card no. 21-1276. The second peak at 2θ = 84.81º corresponds to the (400) plane of the rutile phase, with an intensity of 4% according to the same JCPDS database card. The results indicate that the films are primarily adopting the orientation with the energetically most stable configuration and possible lattice match. If we compare the F82 and F81 films, both obtained at a low total pressure (7.0×10^{-2} mbar), and with comparable thicknesses (354 nm and 294 nm respectively), we observe not only a decrease in peak intensities but also the loss of crystalinity as the argon flux increase from 6 sccm to 30 sccm respectively. Using the Scherrer equation, the average crystallite size of these samples was estimated to drop from 27 nm to 24 nm as the argon flux was raised from 6 sccm to 30 sccm. The rocking curve of the (200) peak for the film grown at Φ_{Ar} = 30 sccm shows a full width at half maximum (FWHM) of 1.51º, a value that is acceptable when compared to values found in the literature.

Optical properties

Figure 5.22 shows the spectral transmittance of the films deposited at two different total

pressures of 5.0×10^{-1} mbar and 7.0×10^{-2} mbar, respectively, for two values of the argon flux, 6 and 30 sccm respectively. It can be seen that the maxima in the transmittance curves decrease as the argon flux is increased in the case of high total pressure (5.0×10^{-1} mbar). This behaviour is probably due to crystalline transition in the films as seen from the X-ray diffraction pattern.

The samples obtained at a total pressure of 7.0×10^{-2} mbar show different characteristics (Fig. 5.22b). When the argon flux is raised up to 30 sccm, the interference pattern in the transmission spectrum shifts to a lower wavelength region, while the transmittance maxima of the films are stable with the argon flux variation.

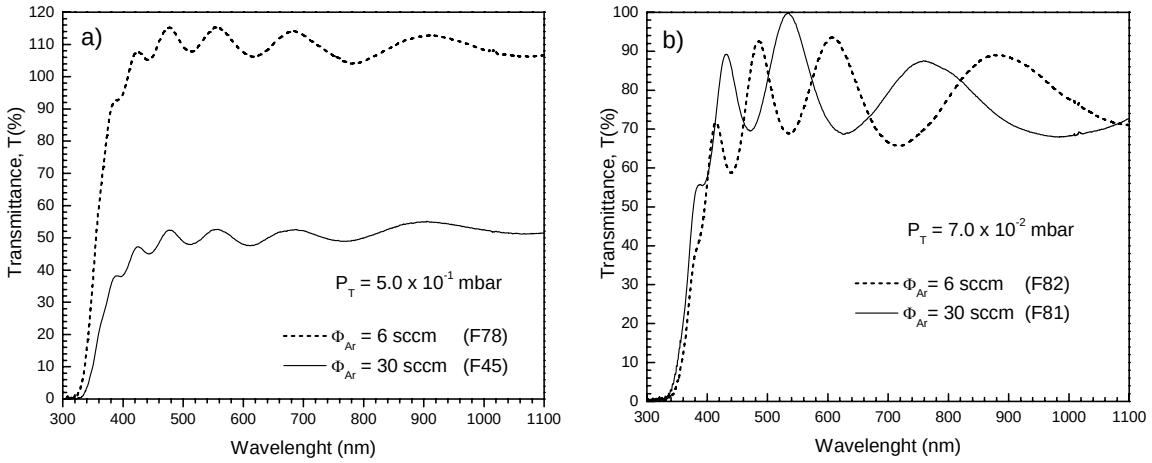

Figure 5.22 Optical transmittance spectra of Co-doped TiO_2 films grown in Ar environment at a) $P_T = 5.0\times10^{-1}$ mbar, b) $P_T = 7.0\times10^{-2}$ mbar.

The indirect band gap energy, E_g^i, was determined for each sample (Fig. 5.23) and the obtained values are shown as a function of argon flow rate in Fig. 5.24. E_g^i decreases with increasing argon flux which means that the absorption edge moves to a lower energy level as the argon content of the backgroung gas increases (the oxygen partial pressure decreases); simultaneously, films become less transparent at the highest argon content.

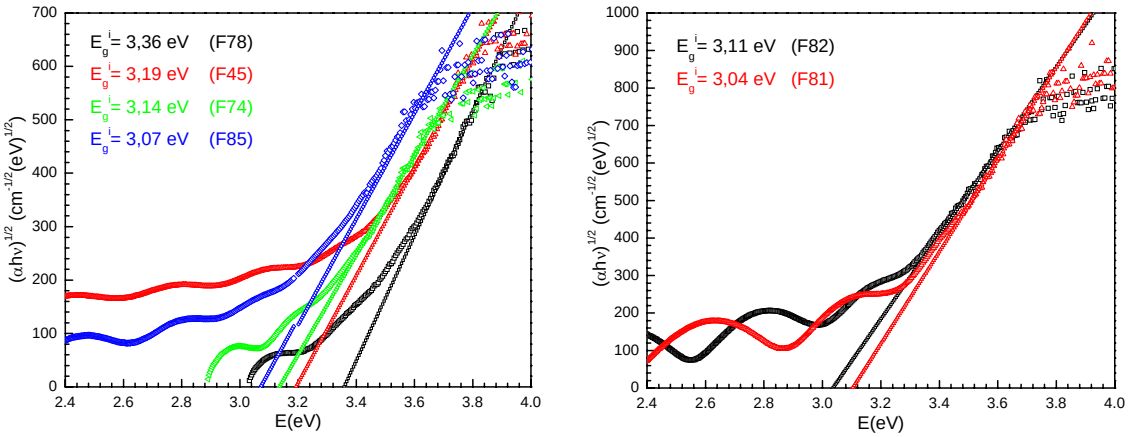

Figure 5.23 Photon energy dependence of the square root of (αhν) for the Co-doped TiO_2 films deposited under the conditions described in Figs. 5.22-a and 5.22-b. Straight lines represent linear fits to the high energy region of the curves. Values for the band gaps of the films are also shown in the figure.

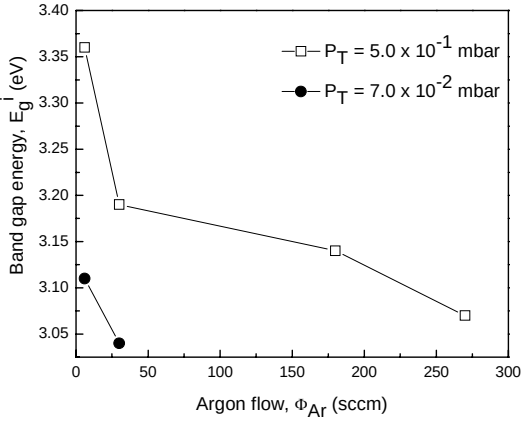

Figure 5.24 Band gap energy, E_g^i, *versus* Ar flux for Co-doped TiO_2 thin films deposited at $P_T = 5.0\times10^{-1}$ mbar and 7.0×10^{-2} mbar, respectively.

5.6 Effect of hydrogen addition and flux (V)

Although not mentioned up to this point in this thesis, we attempted to measure the resistivity of different samples prepared within the experimental series described above. The results were quite disappointing in the sense that all the samples analysed showed evidence of a very high resistivity. In fact, first trials carried out on Co-doped thin films deposited on silicon using oxygen as background gas (samples not included in this thesis report) resulted in extremely high resistivity values. As a consequence, the growth

experiments here reported on sapphire just used argon as buffer gas in an attempt to decrease the resistivity of the samples by creating an oxygen defficient thin film material. It was hoped that the replacement of oxygen with argon in the gas phase would yield the creation and distribution of oxygen vacancies in the Co-doped TiO_2 lattice contributing to ferromagnetic thin films. However, the resistivity of the samples grown within series II (effect of ambient pressure) and IV (effect of argon flux) were still too high, $\rho \sim 6\times10^5$ Ωcm.

Hydrogen is a ubiquitous impurity in most semiconductors, including elemental (e.g. Si), compound (e.g. GaAs) and wide gap semiconductors (e.g. III-V nitrides and II-VIs).[29] In these systems, hydrogen is known to be amphoteric, forming an acceptor level in *n*-type and a donor level in *p*-type materials. In contrast, hydrogen can lead to electron conduction in some wide gap oxides such as SnO_2[30] and ZnO.[31] First-principles total–energy calculation suggests that materials such as Ag_2O, HgO, CuO, PbO, PtO, IrO_2, RuO_2, PbO_2, TiO_2, WO_3, Bi_2O_3, Cr_2O_3, Fe_2O_3, SbO_3, Nb_2O_5, Ta_2O_5, $FeTiO_3$ and $PbTiO_3$ can be doped *n*-type via hydrogen introduction.[32] Therefore, in the following paragraphs we study the effect of hydrogen addition to the gas phase, during the ablation process, upon the growth and properties of the thin films.

Co-doped TiO_2 films were deposited using two substrate temperatures, 200 and 310 ºC. The laser fluence at the target surface was estimated to be 6.4 Jcm^{-2}. A gaseous flow consisting of pure argon or a mixture of argon and hydrogen was let in the chamber during the experiments bringing the total pressure up to 1.0×10^{-1} mbar. The argon flow rate was kept constant at $\Phi_{Ar} = 30$ sccm for both gaseous atmospheres while the hydrogen flow rate, Φ_{H2}, was varied from 0.1 to 1 sccm in the case of the ($Ar+H_2$) environment. The hydrogen flux and substrate temperature are the key parameters for determining the film morphology and consequently the film's properties. The deposition conditions are summarized in table 5.10.

Table 5.10 PLD thin films deposition parameters.

Sample	Laser output energy (mJ)	F (J/cm^2)	T_S (ºC)	P_T (mbar)	Φ_{Ar} (sccm)	Φ_{H2} (sccm)	Number of pulses	Thickness (nm)
F93	157	6.4	310	1.0×10^{-1}	30	0	120 000	1232
F92						0.04		1200
F94						0.1		975
F99						0.2		1008
F90						1		-
F90			200			0.1		928
F98						0.2		858
F100						0.5		800
F101						1		800

Crystal structure

XRD patterns of the films obtained at a substrate temperature of 200 ºC are shown in Fig. 5.25 - a). In case of the sample prepared with 0.1 sccm hydrogen flux, a low intensity (110)

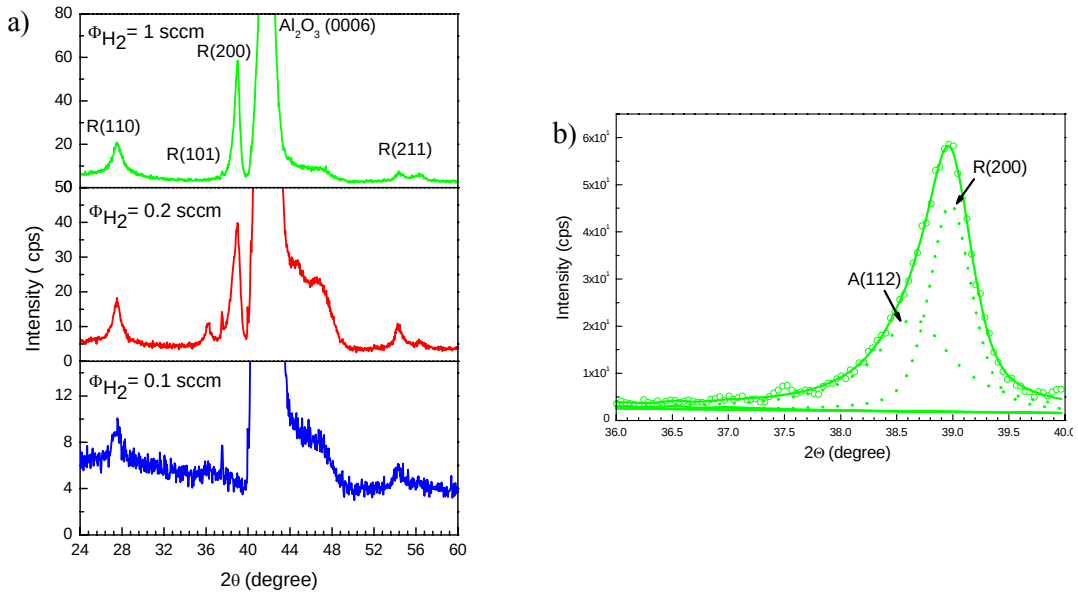

Figure 5.25 (a) XRD patterns of Co-doped TiO_2 thin films deposited on (0001)Al_2O_3 at a total pressure of 1.0×10^{-1} mbar with an argon flow rate of 30 sccm and T_S = 200 ºC. (b) The asymmetric peak at about 2θ = 38.81º was resolved into two peaks: R(200) at 2θ = 38.89º and A(112) at 2θ = 38.65º. Labelled lines were taken from JCPDS file cards no. 21-1272 for anatase and 21-1276 for rutile.

diffraction peak assigned to the rutile phase was noticed. The increase of hydrogen flux to 0.2 sccm results in clear (101), (200), (211) and (220) rutile diffraction peaks. As seen in Fig. 5.25 - b) the 38.81º peak is an asymmetric one due to the convolution of the (200)

rutile and (112) anatase peaks. A careful analysis of this peak using JCPDS database files 21-1272 and 21-1276 yields an intensity of 10% for the anatase phase (112) lattice plane and an intensity of 8% for the rutile phase (200) plane. Anatase phase diminishes at higher hydrogen flow rates as seen in Fig. 5.26 – a). This is in agreement with the fact that low temperatures and rich oxygen environments are favouring the formation of anatase phase. During the deposition process excited oxygen atoms are generated within the laser plume. Since the target has oxygen in excess due to the Co_2O_3 addition, the deposition parameters will influence the amount of oxygen incorporated into the film structure and consequently the relative amount of anatase and rutile phases. At substrate temperatures of 200 ºC, raising the hydrogen flow rate from 0.2 to 1 sccm slightly improves film's crystallinity due to the low reactivity of hydrogen. The FWHM of the (200) rutile line decreases from 0.53º to 0.44º (Fig. 5.26 - a)).

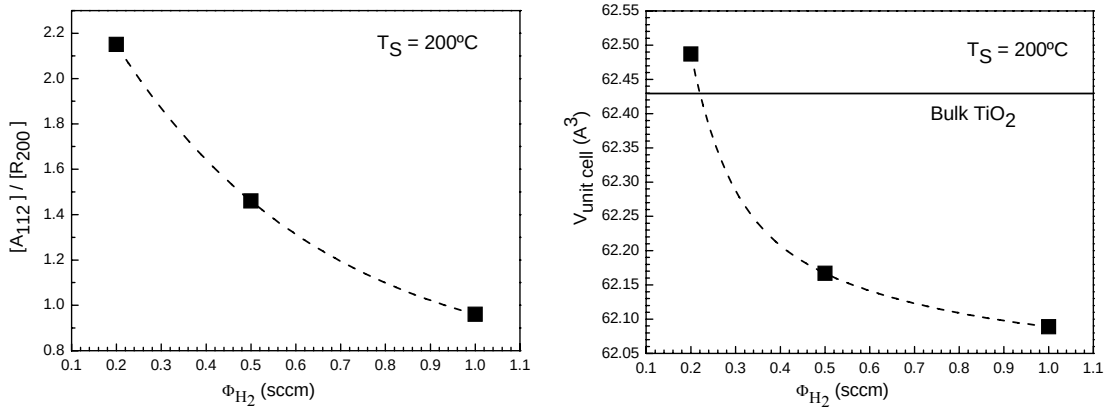

a) b)

Figure 5.26 a) Variation of $[A_{112}]$ / $[R_{200}]$ intensity ratio with hydrogen flux for samples grown at T_S = 200 ºC. b) Volume of the unit cell vs. hydrogen flow rate for the same samples as in a). Dashed lines are for visual guidance only.

Similar film-growth experiments were also performed at a higher substrate temperature, T_S = 310 ºC, and the XRD patterns of these depositions are plotted in figure 5.27. At this temperature, which is much lower than values found in the literature (>500 ºC), formation of the rutile phase is indicated by the presence of the (110), (101), (200) and (211) diffraction peaks. It can be seen that in the absence of hydrogen flux, or for a low flux of 0.1 and 0.2 sccm, the samples present only the (101), (200) and (211) rutile diffraction peaks. The (200) rutile peak is a symmetric one indicating that no anatase phase was formed (Fig. 5.27– b)).

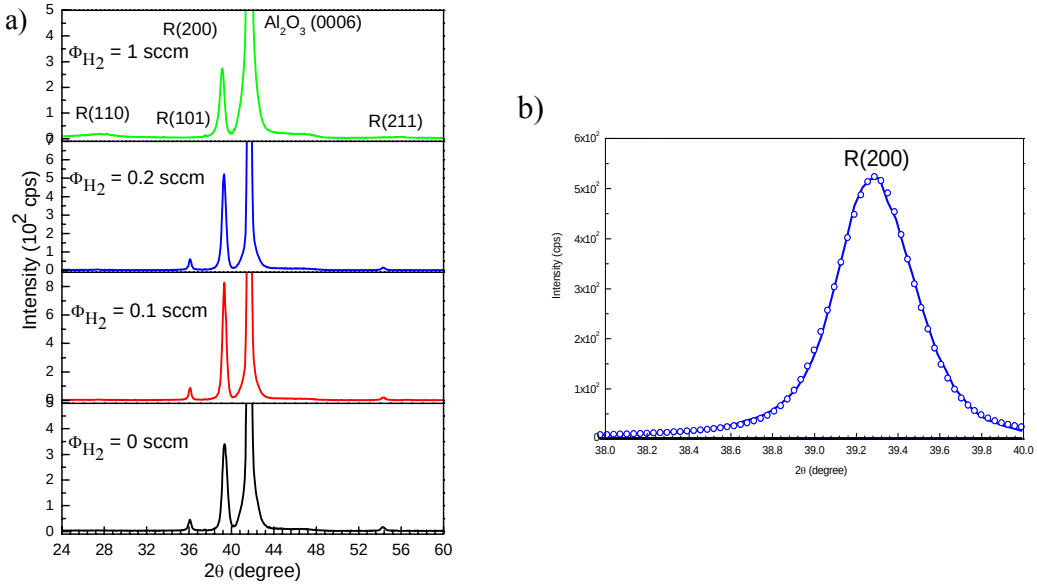

Figure 5.27 a) XRD patterns of Co-doped TiO_2 thin films deposited on (0001)Al_2O_3 at a total pressure of 1.0×10^{-1} mbar with an argon flow rate of 30 sccm and T_S = 310 ºC. b) PsVoigt fit of R(200) at 2θ = 39.29º. The H_2 flow rates are indicated in the figure. Labelled lines were taken from JCPDS file card no. 21-1276 for rutile.

This allows us to conclude that the formation of Co-doped TiO_2 rutile films, highly textured along the [200] direction, is favoured by the decreasing of available oxygen amount and by substrate temperature increasing (see sample with Φ_{H2} = 0 sccm). Film crystallinity was augmented in samples grown with low hydrogen addition 0.1 and 0.2 sccm (FWHM = 0.4º) compared to samples prepared without hydrogen (FWHM = 0.6º). A further increase of the hydrogen flow to 1 sccm led to a slight decrease in film crystallinity (FWHM = 0.5º).

The values of the lattice parameters, calculated from the position of diffraction lines, were found different from the bulk values: lattice parameter *a* is slightly higher, while the *c* lattice parameter is slightly smaller. In case of the samples prepared with a low amount of hydrogen addition, a higher cell volume, $V_{Co:TiO2} = 62.49\times10^{-3}$ nm^3, was obtained compared to that of bulk TiO_2 ($V_{TiO2} = 62.43\times10^{-3}$ nm^3). This can be explained by the substitution of Ti^{4+} having an ionic radius of 0.064 nm in the rutile lattice with the Co^{2+} that has a larger ionic radius of 0.082 nm. By increasing the hydrogen concentration in the deposition atmosphere a monotonic decrease of volume cell was observed. This variation in lattice constants is related to oxygen deficiency induced by the presence of hydrogen molecules. Upon reduction, oxygen vacancies are introduced, giving rise to a significant

change in films properties. The defects result in n-type doping due to the donor levels in the band gap. Oxygen vacancies form color centers which trap electrons at 0.76 eV below the conduction band and change the color of the crystal from transparent through light grey to dark grey (sample grown at $\Phi_{H2} = 1$ sccm).

Optical properties

The optical transmittance spectra of the as-deposited Co-doped TiO_2 films, recorded in the wavelenght range from 300 to 1100 nm are plotted in figure 5.28. The average value of transmittance in the visible region, <T>, decreases by adding hydrogen to the ambient gas. For the samples prepared at $T_S = 310$ ºC, <T> decreases from 85% in case of the film prepared in pure argon to 54% for the film prepared with 0.2 sccm H_2; at a substrate temperature of $T_S = 200$ ºC, the corresponding decrease is from 100% for the sample prepared with 0.1 sccm H_2 to 20% for the film prepared with an hydrogen flow rate of 1.0 sccm. This behaviour is also accompanied by the change of the visual aspect of the films from highly transparent (e.g., samples F93 and F96) to less transparent dark-grey ones (e.g., samples F90 and F101). Indeed, the transmittance of sample F90 could not be measured, the sample being completely dark and absorbant.

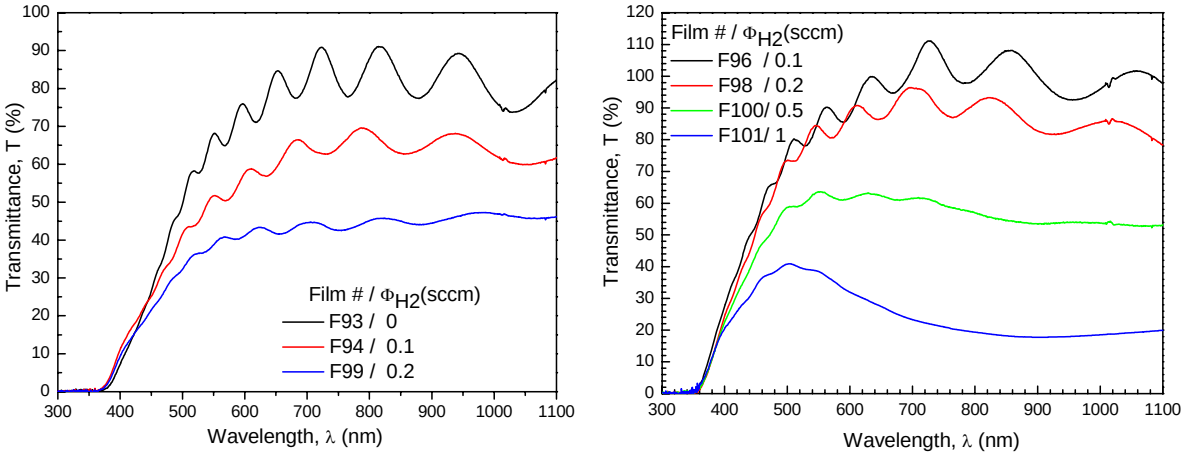

Figure 5.28 Optical transmittance spectra of Co:TiO_2 films grown in Ar/H_2 environment at 1.0×10^{-1} mbar, for various H_2 flow rates; substrate temperature: $T_S = 310$ ºC (left) and $T_S = 200$ ºC (right).

The transmittance reduction can be explained by two mechanisms:

(a) the increase of surface light scattering due to augmentation of surface roughness caused by improved crystallinity;

(b) the change of Ti charge state from Ti^{4+} to Ti^{3+} taking place in order to maintain lattice charge neutrality; this might occur for some Ti atoms accompanying the decrease of the number of oxygen atoms incorporated in the films during deposition.[33] We will come back to this hypothesis later when we will discuss the results obtained by XPS.

The thickness of the films, *d*, was calculated from the optical transmission measurements, T(%), using equation (4−16). Assuming that intensity losses due to reflection may be neglected, the optical absorption coefficient α, was calculated using equation (4−17).

Figure 5.29 displays Tauc plots[34] of $(\alpha h\nu)^{1/2}$ versus hν. The high energy portion of the curves was fitted by straight lines which were extrapolated to zero absorption giving the indirect band gap energies, E_g^i, for the different samples deposited at T_S = 310 ºC: 2.85 eV for the film deposited with pure argon atmosphere (film F93), 2.77 eV and 2.72 eV for the films grown with hydrogen assistance, respectively 0.1 and 0.2 sccm. For the samples grown at T_S = 200 ºC, the indirect band gap energies, E_g^i, are 3.05 eV for the film deposited at low hydrogen flow (sample F96, Φ_{H2} = 0.1 sccm), 2.94 eV, 2.81 eV and 2.78 for the films obtained with Φ_{H2} = 0.2, 0.5 and 1 sccm.

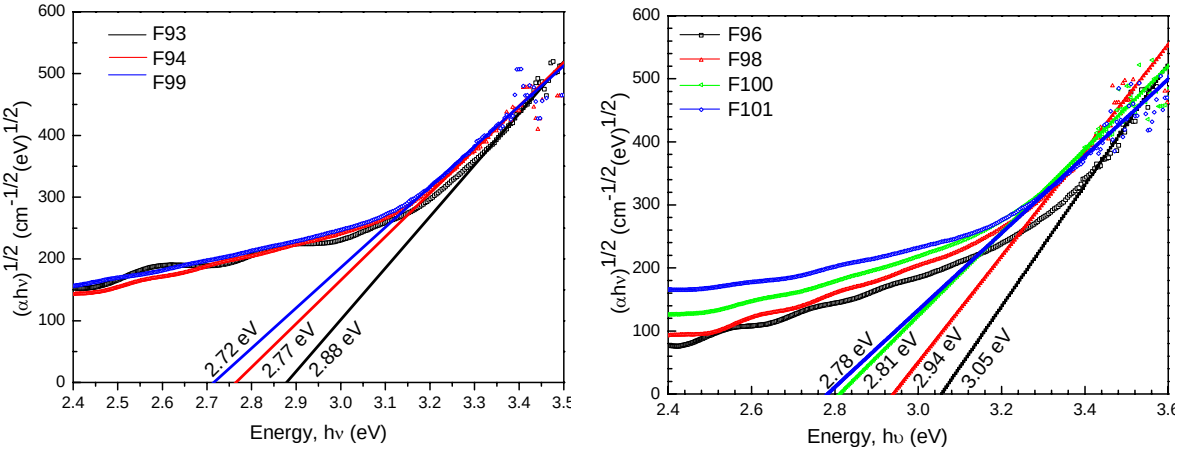

Figure 5.29 Photon energy dependence of SQRT (αhν) for the Co-doped TiO_2 films deposited under the conditions described in Fig. 5.28. Straight lines represent linear fits to the high energy region of the curves. Values for the band gap of the films are also shown in the figure.

If these values are compared with that for pure TiO_2 rutile films (E_g^i = 3.05 eV), it can be concluded that the optical band gaps shift to the red in the Co-doped rutile films, a result consistent with n-type doping of the materials. Moreover, it is clearly seen that the onset of

the absorption edge shifts to higher wavelength values (red shift) when hydrogen is added to the argon environment during deposition, and that this increase is proportional to the hydrogen content of the background gas phase. This result indicates that the addition of a small amount of hydrogen is effective for the promotion of oxygen vacancies whereby states are introduced just below the conduction band, as expected.

The optical transmission measurements were complemented by spectroscopic ellipsometry (SE) characterisation of the samples. A Horiba-Jobin Yvon UVISEL spectroscopic ellipsometer working in a wide energy range 0.59 − 6.50 eV was used. However, the experimental results were fitted within a shorter range (1.0 – 5.0 eV) since the available Co reference was limited to this energy range. The incidence angle was kept at 70º.

The fitting procedure requires a model to describe the layered structure of the deposited material. This is schematised in Fig. 5.30: substrate (Al_2O_3); incubation layer consisting of Co-doped TiO_2 + 10% voids; bulk (Co-doped TiO_2); surface layer consisting of Co-doped TiO_2, voids and Co clusters.

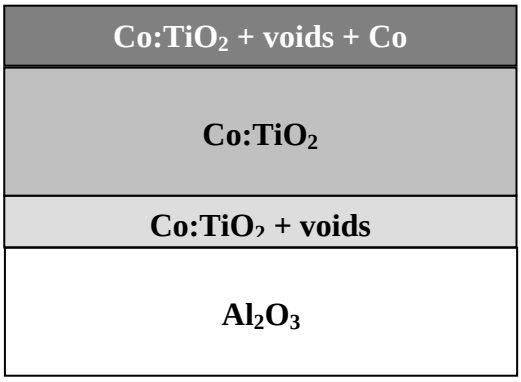

Figure 5.30 Layered structure model used to fit the SE data

The film material was fitted using the Tauc-Lorentz-Drude (TLD) model, while the surface properties where obtained by fitting the surface layer with a Bruggeman Effective Medium Approximation (BEMA) of TLD, voids, and Co reference. The TLD model comprises the Tauc-Lorentz oscillator, which combines the Tauc band edge with the classical Lorentz broadening function[35]. Here, five parameters are required to describe the real, ε_1 and imaginary, ε_2 parts of the dielectric function of the material:

$$\varepsilon_1(E) = \varepsilon_1(\infty) + \frac{2}{\pi} P \int_{E_g}^{\infty} \frac{\varepsilon_2(u)}{u^2 - E^2} du \quad (5\text{-}1)$$

$$\varepsilon_2(E) = \frac{AE_0C(E - E_g)^2}{(E^2 - E_0^2)^2 + C^2E^2} \frac{1}{E} \quad (5\text{-}2)$$

where A is the transition matrix element, normally related with the density of the material, E_0 the peak transition resonance energy, E_g the optical band gap and C the broadening parameter that is inversely related with the short range order[36,37]. $\varepsilon_1(\infty)$ is a fitting constant to prevent ε_1 from converging to zero for energies below the band gap.

The Drude free electron[38] oscillator describes the refractive index, *n*, and extinction coefficient, *k*, behaviour in the near-infrared due to the free electrons in the material:

$$\tilde{\varepsilon}(\omega) = \varepsilon_\infty + \frac{\omega_P^2}{-\omega^2 + i\Gamma_d\omega} \quad (5\text{-}3)$$

where ω_P is the plasma frequency and Γ_d is the broadening term. The plasma frequency, ω_P, is proportional to the free electron density, while Γ_d is inversely proportional to the free charge carrier mobility.

The layered structure model shown previously was the simplest one that could provide a low enough error, ($\chi^2 \leq 1$) between experimental data and the model. In most of the cases, this model was simplified to just two layers, as the fitting provided an incubation layer of zero thickness. This result shows that the bulk of the films is homogeneous along their thickness.

The refractive index, *n*, and extinction coefficient, *k*, of the bulk layer of the Co-doped TiO_2 are shown in figure 5.31, and the thickness of the layers is shown in table 5.11. We have tried to fit the bulk layer introducing also a small percentage of Co clusters, but the best fit was obtained for a 0 % value. This means that no Co clusters were present in the bulk of the films and, therefore, all the Co atoms are substituting the Ti in the TiO_2 lattice.

The films grown with low Φ_{H2} present an index, *n*, of 2.34 at 1.5 eV, very close to the 2.4 found by others in non-doped rutile TiO_2 films deposited by PLD[39]. On the other hand, the peak E_0 is more intense in our Co-doped TiO_2 films ($4<n<6$) than in those from ref.[39]. The gap, E_g determined by the TLD model is always lower than the real optical (Tauc plot) gap

since it corresponds to the energy of k = 0 eV. This gap does not match the real optical gap of amorphous or nanocrystalline materials, where band tails exist, and the edge of absorption should be defined by the Tauc plot[34]. Using the Tauc plot method a value 2.8 eV was found[40], which is lower than the 3.3 eV found for the non doped TiO_2[39]. These results show that the Co-doped TiO_2 films have a density similar to the non doped TiO_2, but the Co, which can distort the network, and the addition of oxygen vacancies due to the presence of H_2 in the background gas, must create some density of states in the gap, that lowers E_g and increases optical absorption, while the index, *n*, slightly reduces.

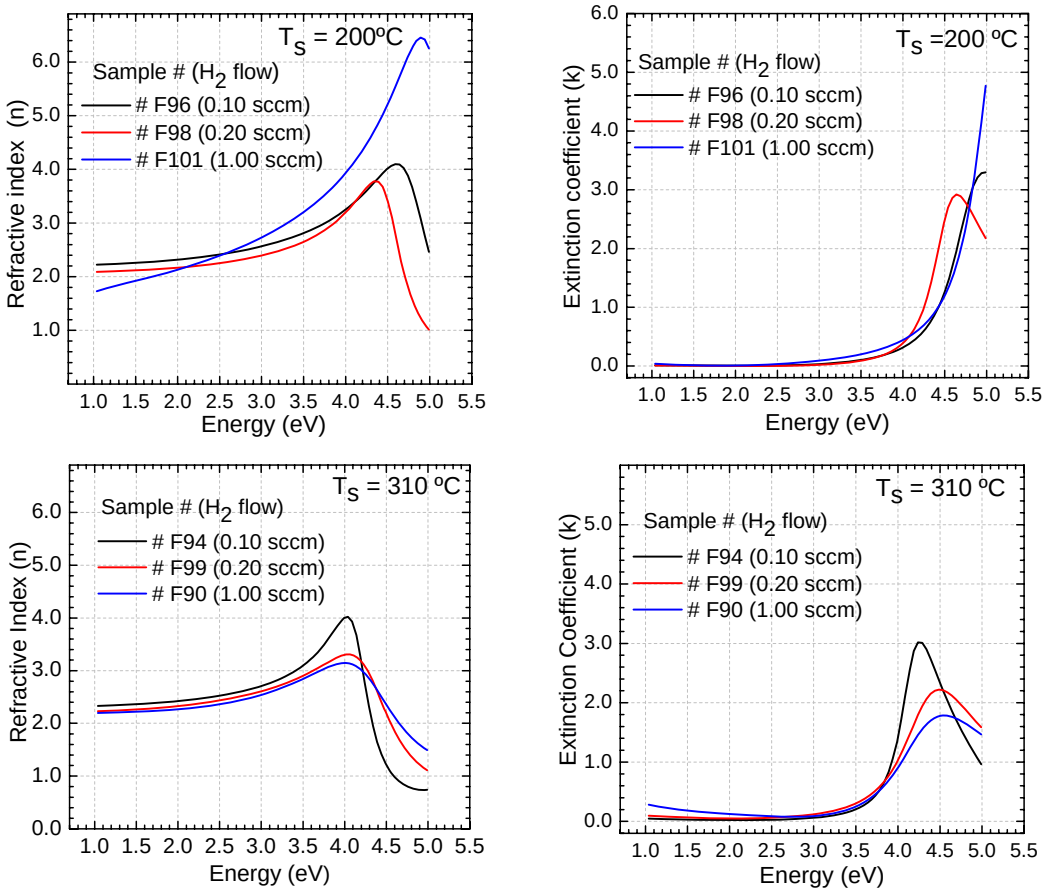

Figure 5.31 Refractive index (left panels) and extinction coefficient (right panels) of the bulk layer of the Co-doped TiO_2 films, as a function of H_2 flow rate for two substrate temperatures, T_S.

The increase of Φ_{H2} and T_S, all lead to an increase of the optical absorption by the films. This is observed in the decrease of *n* and increase of *k* in the red and near infrared region (< 2 eV), as Φ_{H2} and T_S increase. The main cause of this behaviour is most likely the increase of oxygen vacancies caused by the H_2 dilution and substrate temperature, leading the films to become more metallic and less dielectric. The most metallic film was obtained

at 310 ºC using 1.0 sccm of H_2 dilution, in agreement with the optical transmission measurements discussed above. This film presented a dark metallic appearance. The less metallic films were deposited with T_S = 200 ºC, H_2 = 0.10 sccm and T_S = 310 ºC, H_2 = 0.0 sccm. For these films *k* was 0 in the near infrared region. Table 5.11 shows the ω_p and Γ_d parameters, extracted from the Drude model. The higher the ω_p, the higher the density of free electrons, while the lower the Γ_d, the higher the mobility of the free electrons.

Concerning the film's surface, it is observed that the *n* on the surface is lower and the *k* is higher in comparison with the bulk of the films. This indicates that at the film's surface the density of free electrons is higher than in the bulk. The *n* and *k* of the surface are shown in Fig. 5.32 and the fitting results in table 5.11.

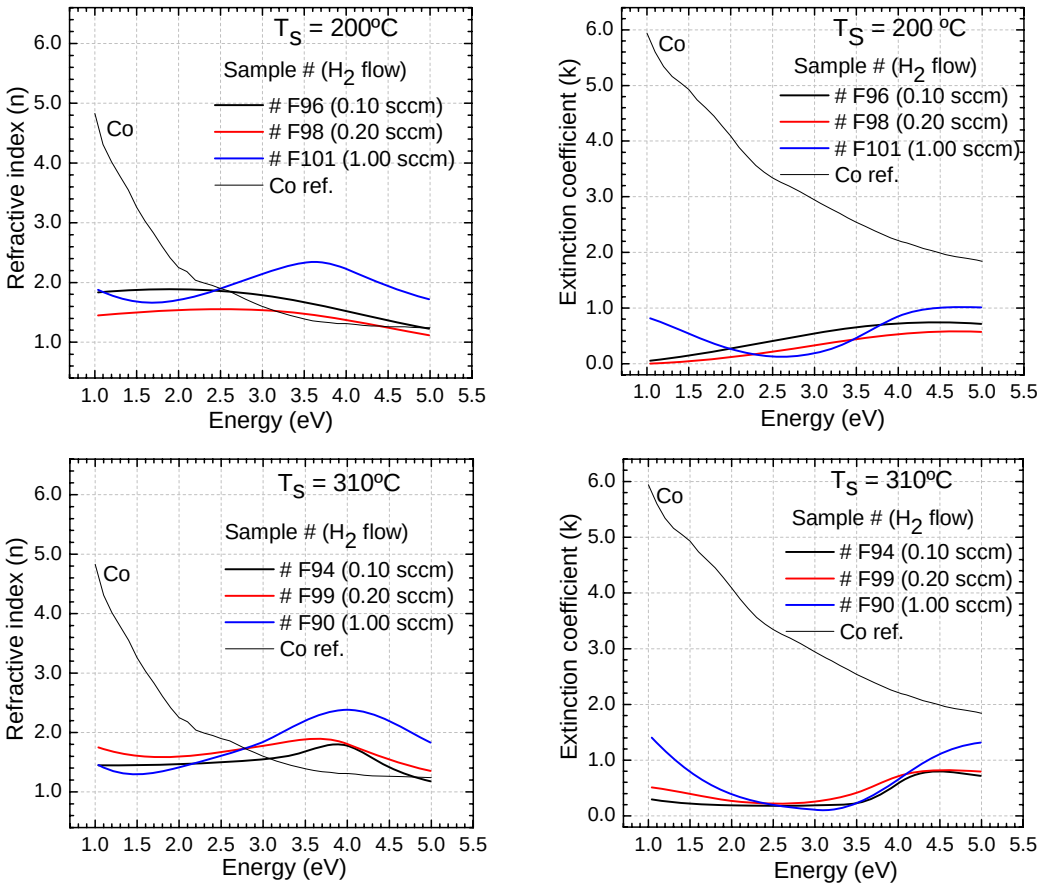

Figure 5.32 Refractive index (left panels) and extinction coefficient (right panels) of the surface layer of the Co-doped TiO_2 films, as a function of H_2 flow rate for two substrate temperatures, T_S.

For some of the Co-doped TiO_2 films, the results indicate that Co segregated to the surface and formed cluster precipitates at the surface. This precipitation seems to be dependent on

Table 5.11 Parameters of the Tauc-Lorentz and Drude dispersions obtained from the fitting of the bulk layers of the films. Thickness of the layers in the model, percentage of Co in the surface layer and error χ^2 of the fitting.

Sample	H_2 (sccm)	Ts (ºC)	ε^{∞}	Eg (eV)	A	E_0 (eV)	C	ω_P (eV)	Γ_d	Incubation thick. (nm)	Bulk thick. (nm)	Surface thick. (nm)	% Co in surface	χ^2
F96	0.10	200	2.26	2.19	45.60	4.80	0.64	0.00	∞	0	947	73	1.76	0.962
F98	0.20	200	2.52	2.32	36.48	4.51	0.50	0.27	1.71	0	1012	66	0.00	1.158
F100	0.50	200	-1.06	1.89	73.22	4.90	0.44	0.84	1.27	93	604	61	0.11	0.566
F101	1.00	200	-3.84	1.81	94.25	5.07	0.61	0.85	0.21	71	554	38	0.38	0.673
F93	0.00	310	2.88	2.04	35.99	4.36	0.37	0.00	∞	0	1235	66	6.94	1.109
F92	0.04	310	2.83	2.04	37.88	4.48	0.56	0.62	2.43	0	1215	52	13.12	0.526
F94	0.10	310	3.58	1.87	25.83	4.16	0.41	2.14	20.17	0	1020	38	5.49	0.509
F99	0.20	310	2.95	1.77	26.57	4.31	0.80	4.74	50.07	0	1088	37	1.51	0.377
F90	1.0	310	3.11	2.58	56.51	4.29	1.03	2.47	4.51	0	1121	11	0.00	0.212

T_S, which is typical of a temperature dependent diffusion mechanism. On the other hand, as will be shown later[39], for T_S= 310 ºC the films display a superparamagnetic behaviour indicative of Co nanoclustering, which agrees well with the SE results here presented.

Surprisingly, the Co cluster % at the surface decreases with the H_2 dilution, which does not mean that there is less Co at the surface, but means that it did not precipitate and did not form clusters, probably due to the oxygen vacancies created by the H_2. The films deposited in these conditions (F99 and F90) exhibit a different optical behaviour from the rest, indicating a different morphology. The Tauc-Lorentz C parameter is high in these films, meaning a broader structure, expected from an oxide with a high concentration of oxygen vacancies. On the other hand, the higher *k* in the bulk layer also indicates a more metallic behaviour, which could be related to Co incorporation in the bulk, which has valence 2, in contrast with the valence 4 of Ti, creating two free electrons as it incorporates.

Chemical analysis by RBS, ERDA and XPS

The RBS spectra of the Co:TiO_2 samples grown with hydrogen assistance were recorded using the same experimental conditions as for previous series. The results for the sample F94 (310 ºC, 0.1 sccm H_2) and the corresponding curve fit are displayed in figure 5.33-a). Again, the shape of this spectrum indicates that the film is homogeneous along depth (Ti profile is approximately flat) and that the diffusion of the Co is relatively uniform.

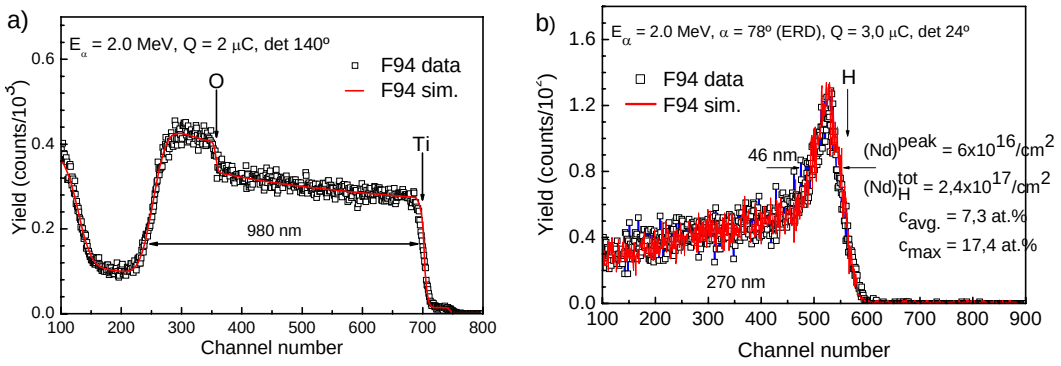

Figure 5.33 a) RBS and b) ERDA spectra of sample F94 recorded for $^4He^+$ incident energy of 2 MeV and the corresponding theoretical simulations.

As the samples of this series were deposited in H_2 environment, we expected the samples to be oxygen deficient and to contain some amount of hydrogen; for this reason, elastic recoil detection analysis (ERDA) was also performed, in particular for sample F94 (Fig. 5.33-b), allowing for the determination of the hydrogen content in the samples.

The chemical composition and thickness of sample F94 evaluated with the RUMP simulation of the RBS spectrum, recorded with α particles, were $Ti_{0.965}Co_{0.035}O_{1.965}$ and 855 nm (using the density of rutile), respectively. After H_2 content correction obtained by ERDA, these values were corrected to $Ti_{0.965}Co_{0.035}O_{1.965}H_{0.3}$ and 930 nm.

X-ray photoelectron spectroscopy (XPS) was used for both composition evaluation and chemical bonding analysis. The main features of XPS technique were described in section 4.3.4. In this work, XPS analysis was carried out using an XSAM800 spectrometer from Kratos. The binding energies of the various photoelectron peaks were calibrated with respect to the C 1s peak taken at 284.8 eV. This peak comes from contamination of the film surface with hydrocarbons to which XPS is highly sensitive. Peak fitting was made using the software package associated to the spectrometer. The first step consisted on background subtraction using a Shirley + linear type funcion; afterwards, the spectra were fitted using Lorentzian-Gaussian peak shapes. The results obtained are presented in table 5.12 for samples grown at 310 ºC without hydrogen (F93) and with 0.2 sccm H_2 (F99).

Table 5.12 XPS results in the Co 2p and Ti 2p core level regions.

Peak	Position (eV)	FWHM (eV)	Raw area	Sensitivity factor	Atomic mass	At.%	Wt.%
Sample F93							
Ti 2p	458.60	1.43	19209	1.800	47.9	84.50	81.59
Co 2p	781.50	2.46	7441	3.800	58.9	15.50	18.41
Sample F99							
Ti 2p	458.80	1.42	16180	1.800	47.9	78.18	74.45
Co 2p	781.30	3.99	9535	3.800	58.9	21.82	25.55

The binding energy of Ti $2p_{3/2}$ was determined to be at approximately 458.60 eV (sample F93) and 458.80 eV (sample F99) and therefore the Ti peak can be assigned to the Ti^{4+} (TiO_2) in very reasonable agreement with the literature[41,42]. No evidence of the presence of Ti^{3+} was noticed and thus the change of Ti charge state from Ti^{4+} to

Ti^{3+} to compensate from the lacking of oxygen ions can be discarded.

The core level of Co $2p_{3/2}$ for our samples is at 781.50 eV and 781.30 eV respectively for sample F93 and sample F99. Fa-Min Liu *et al.*[12] found a core level of Co $2p_{3/2}$ @ 782.2 eV in their samples (Co-TiO_2 anatase sandwich) and by comparing their results with those of ref.[43] concluded that the Co was in metal state in the anatase TiO_2. In our films, the binding energy of Co $2p_{3/2}$ peak occurs at lowerr values demonstrating that there is an interaction between the Co ions and their TiO_2 neighbours.

Because XPS is a surface probing technique, the obtained concentrations just concern a surface layer, a few nanometers thick. From table 5.12 and the film stoichiometry determined with RBS, it can be concluded that the [Co]/[Ti] ratio is higher in this surface layer than in the bulk of the thin films which agrees well with the SE measurements.

Electrical and magnetic properties

As demonstrated by the XRD patterns, when the titanium dioxide is treated so as to cause a loss of oxygen in the lattice by the addition of a very small amount of hydrogen, the crystallinity of the film increases. When the H_2 concentration becomes too high, the hydrogen reacts not only at the surface but also inside the structure, creating disorder. This can be seen for the film obtained at 310 ºC and Φ_{H2} = 1 sccm, which displays a relatively uniform surface structure (Fig. 5.34) consisting of clusters of very small grains (quasi-amorphous structure).

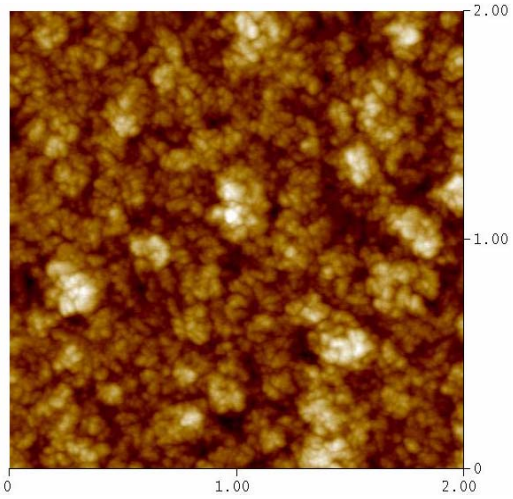

Figure 5.34 AFM image (2.0 μm×2.0 μm) of the surface morphology of a Co-doped TiO_2 film deposited at T_S = 310 ºC and Φ_{H2} = 1 sccm

The film surface is rendered smoother by increasing the hydrogen flux at both substrate temperatures. For electronic applications, the roughness will significantly influence the utility of films grown using H_2. Films deposited with hydrogen showed an apparent increase in oxygen vacancies, based on the dark coloration of the films and increased conductivity. For samples obtained at both substrate temperatures, 200 ºC and 310 ºC, the resistivity decreases as the hydrogen flow rate increases (Fig. 5.35, inset):

a) from 1.9 Ωcm to 0.7 Ωcm at T_S = 200 ºC, and

b) from 0.9 Ωcm to 0.1 Ωcm at T_S = 310 ºC.

The measured resistivity of the film grown at T_S = 310 ºC and Φ_{H2} = 0 sccm is very high compared to that of the films deposited with hydrogen addition. This reflects the fact that the electrical properties depend very strongly on the density of oxygen vacancies and surface roughness.

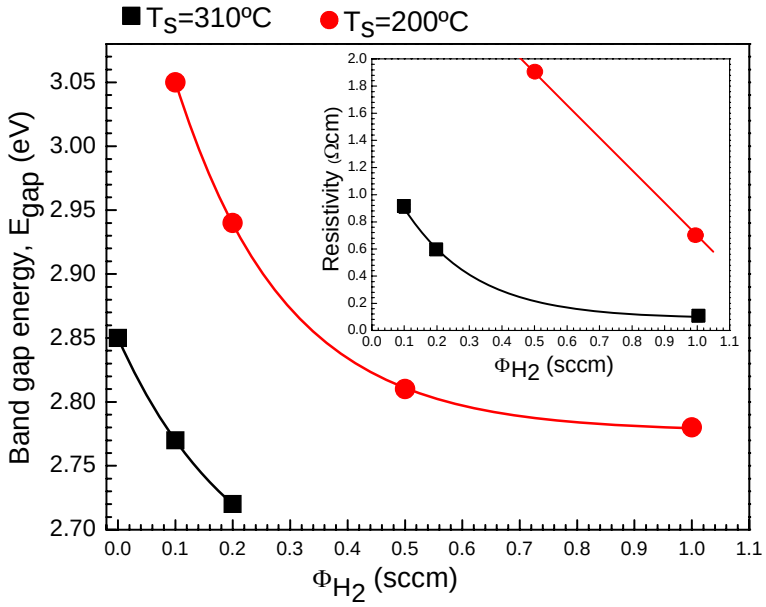

Figure 5.35 Band gap energy as a function of hydrogen flow rate. Inset: resistivity *vs*. hydrogen flux

Finally, the magnetic properties were studied with respect to oxygen vacancy. Similarly to the resistivity measurements, only the films deposited at 310 ºC with hydrogen assistance gave a magnetic signal in a Vibrating Sample Magnetometer (VSM) apparatus. Figure 5.36-a) shows the hysteresis curves, *M(H)*, of the sample

F94, recorded for a magnetic field applied parallel to the film plane and varying up to 5 T, in a wide range of temperature, between 10 K and 300 K (room temperature). The saturation magnetization, M_S, values were deduced from the high-field region of the hysteresis loops and are plotted as a function of temperature in Fig. 5.36-b). As can be seen, M_S decreases from 0.84 μ_B/Co ion at 10 K to 0.25 μ_B/Co at RT.

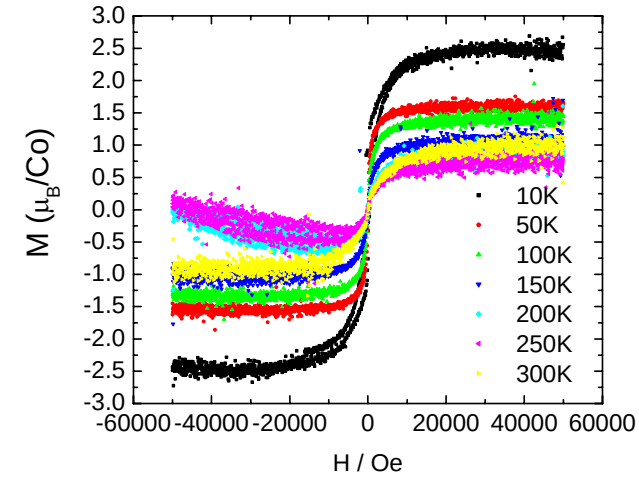

a)

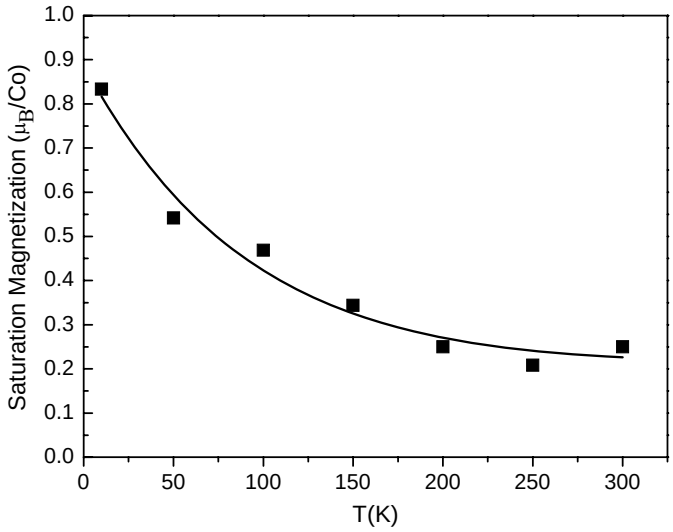

b)

Figure 5.36 a) Magnetization $M(\mu_B$/formula unit) *versus* applied magnetic field for sample F94 (T_S = 310 ºC, $P_T = 1.0\times10^{-1}$ mbar, Φ_{Ar} = 30 sccm and Φ_{H2} = 0.1 sccm), recorded at various temperatures; b) Saturation magnetization, M_S, as a function of temperature. The solid line is provided as a visual guide.

The $M_S - T$ curve can be looked upon as resulting from the superposition of a fast decreasing component at low temperature, indicative of a paramagnetic behaviour,

and a rather flat one at > 200 K. The latter clearly assumes a value different from zero and can be assigned to a ferromagnetic contribution with a Curie temperature higher than 300 K. Therefore, a possible explanation for this temperature dependence could be the presence of Co nanoclusters in parallel with Co ions dissolved in the titania matrix.

Recently, Magnetic Circular Dichroism (MCD) in the spectral region close to the ZnO band edge at ~3 eV was used to show that 300 K ferromagnetism in doped ZnO films is intimately connected with the ZnO band electrons, and that the carriers are polarised[44]. A measurement of MCD at photon energy E gives the difference in absorption for left and right circularly polarized light at that same energy, providing a clear indication of the extent to which the states involved in the transition at that particular energy are influenced by the magnetism. Hence it was hoped that MCD studies might help resolve the issue in Co:TiO2 films. A few samples were studied by magneto-optic spectroscopy in the spectral region around the band edge of the titania films (~ 3 eV) by illuminating the samples with a xenon lamp. Figure 5.37 shows the results obtained at 10 K in a field of 0.45 T for a film grown at 310 ºC with 0.5 sccm H_2 / 30 sccm Ar.

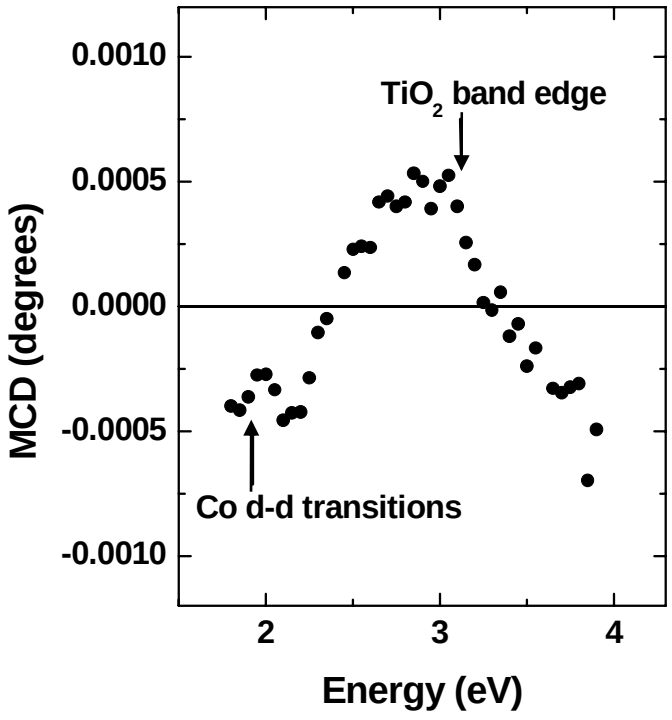

Figure 5.37 MCD of a 2.1μm thick film on an (0001) Al_2O_3 substrate, at 10 K in a field of 0.45 T

The arrows indicate the Co d-d transitions at 2 eV and the band edge for bulk TiO_2 at 3.05 eV. The broad peak centered at ~ 2.8 eV, which corresponds to the band edge measured for equivalent thin films, is indicative of the magnetic ions hybridizing with the TiO_2 conduction band causing spin splitting of the latter one. The width of this peak is attributed to the oxygen vacancy impurity band broadening the peak.

Therefore, while the presence of Co-nanoclusters in the films cannot be eliminated, the presence of a reduced band energy with associated magnetic circular dichroism is consistent with spin splitting of the TiO_2 conduction band indicating that the observed magnetic behaviour is directly associated with the titania lattice.

More recently, SQUID measurements performed on a couple of samples, including film F94, showed a well defined broad peak centered at ~ 17 K being observed in the *M(T)* curve recorded in zero field cooling conditions. This temperature can be associated with a blocking temperature. Moreover, the magnetization exhibited a fast decay approaching zero at 300 K. These results led to the conclusion that the samples are superparamagnetic, contradicting the VSM and MCD ones. However, as pointed out by J.M.D. Coey there is a problem of stability of this type of samples where the moment is often unstable in time. The author showed[45] that the moment tends to decay if the same sample is measured on successive occasions, with a characteristic decay time of weeks or months. This might explain the differences encountered above.

5.7 References

1. J.-H. Kim, S. Lee, H.-S. Im, "The effect of target density and its morphology on TiO_2 thin films grown on Si(100) by PLD", Appl. Surf. Sci. 151 (1999) 6-16
2. T. Yamaki, T. Sumita, S. Yamamoto, A. Miyashita, "Preparation of epitaxial TiO_2 films by PLD for photocatalyst applications", J. Cryst. Growth 237 (2002) 574
3. L.R. Doolittle, "Algorithms for the rapid simulation of Rutherford backscattering spectra", Nucl. Instr. and Meth. in Phys. Res. B 9 (1985) 344
4. J.-H. Kim, S. Lee, H.-S. Im, "The effect of different ambient gases, pressures, and substrate temperatures on TiO_2 thin films grown on Si(100) by laser ablation

technique", Appl. Phys. A 69 (1999) S629-S632

5. P. M. Huppertz, D. Mergel, "Nucleation and growth in TiO_2 films prepared by sputtering and evaporation", Thin Solid Films 251, (1994) 72
6. K. Okimura, A. Shibata, N. Maeda, K. Tachibana, Y. Noguchi, K. Tsuchida, "Preparation of rutile TiO_2 films by RF magnetron sputtering", Jpn. J. Appl. Phys. 34 (1995) 4950
7. A. Shibata, K. Okimura, Y. Yamamoto, K. Matubara, "Effect of Heating Probe on Reactively Sputtered TiO_2 Film Growth", Jpn. J. Appl. Phys. 32 (1993) 5666
8. B.D. Cullity and S.R. Stock, "Elements of X-ray Diffraction", 3rd edition, Prentice-Hall Inc., New Jersey, 2001, p. 170
9. A. Ohmori, K.C. Park, M Inuzuka, Y. Arata, K. Inoue, N. Iwamoto, "Electrical conductivity of plasma-sprayed titanium oxide (rutile) coatings", Thin Solid Films 201 (1991) 1
10. J.R. Simpson, H.D. Drew, S.R. Shinde, R.J. Choudhary, S.B. Ogale, T. Venkatesan, "Optical band-edge shift of anatase $Ti_{1-x}Co_xO_{2-\delta}$", Phys. Rev. B 69 (2004) 193205
11. W.K. Park, R.J. Ortega-Hertogs, J.S. Moodera, Alex Punnoose, M.S. Seehra, "Semiconducting and ferromagnetic behavior of sputtered Co-doped TiO_2 thin films above room temperature", J. Appl. Phys. 91 (2002) 8093
12. Fa-Min Liu, Tian-Min Wang, J.Q. Li, Y.Q. Zhou, M.C. Zhang, "Optical and magnetic properties of Co-TiO_2 sandwich composite films grown by magnetron sputtering", submitted to Journal of Crystal Growth
13. A. Sambri, M. Radovic, X. Wang, S. Amoruso, F. Miletto Granozio, R. Bruzzese, "Substrate heating effects on the propagation dynamics of laser produced plume during pulsed laser deposition of oxides", Appl. Surf. Sci. 254 (2007) 790
14. E. Ritter, " Deposition of oxide films by reactive evaporation", J. Vac. Sci. Technol., 3 (1966) 225
15. H. Küster and J. Ebert, "Activated reactive evaporation of TiO_2 layers and their absorption indices", Thin Solid Films 70 (1980) 43
16. D.B. Chrisey and G.K. Hubler (eds.), "Pulsed Laser Deposition of Thin films", New York, Wiley, 1994
17. D.B. Geohegan, A.A. Puretzky, G. Duscher, S. Pennycook, Appl. Phys. Lett. 72 (1998) 2987
18. H.W. Kroto, J.R. Heath, S.C. O'Brien, R.F. Curl and R.E. Smalley, Nature 318

(1985) 162–163

19. M. Becker, J. Brock, H. Cai, D. Henneke, J. Keto, J. Lee, W. Nichols, H. Glicksman, Nanostruct. Mater. 10 (1998) 853–863
20. M. von Allmen, Laser–Beam Interactions With Materials: Physical Principles and Applications (Berlin: Springer) 1987
21. S.S. Harilal, C.V. Bindhu, V.P.N. Nampoori, C.P.G. Vallabhan, "Influence of ambient gas on the temperature and density of laser produced carbon plasma", Appl. Phys. Lett. 72 (1998) 167–169
22. S.S. Harilal, "Expansion dynamics of laser ablated carbon plasma plume in helium ambient", Appl. Surf. Sci. 172 (2001) 103–109
23. D.B. Geohegan, "Diagnostics and characteristics of pulsed laser plasmas", in Pulsed Laser Deposition of Thin Films, edited by D.B. Chrisey and G.K. Hubler, Wiley, New York, 1994, pp. 115–165
24. D.B. Geohegan and A.A. Puretzky, "Dynamics of laser ablation plume penetration through low pressure background gases", Appl. Phys. Lett. 67 (1995)197–199
25. A.V. Bulgakov and N.M. Bulgakova, "Dynamics of laser-induced plume expansion into an ambient gas during film deposition", J. Phys. D: Appl. Phys. 28 (1995)1710–1718
26. A.V. Bulgakov and N.M. Bulgakova, "Gas-dynamic effects of the interaction between a pulsed laser-ablation plume and the ambient gas: analogy with an under expanded jet", J. Phys. D: Appl. Phys. 31 (1998) 693–703
27. R.F. Wood, J.N. Leboeuf, K.R. Chen, D.B. Geohegan, A.A. Puretzky, "Dynamics of plume propagation, splitting, and nanoparticle formation during pulsed-laser ablation", Appl. Surf. Sci. 127–129 (1998) 151–158
28. A.V. Rode, E.G. Gamaly, B. Luther-Davies, "Formation of cluster-assembled carbon nano-foam by high-repetition-rate laser ablation", Appl Phys A 70 (2000) 135–144
29. S.K. Estreicher, "Hydrogen-related defects in crystalline semiconductors: a theorist's perspective", Mater. Sci. Eng. R. 14 (1995) 319.
30. S. Samson, C.G. Fonstad, "Defect structure and electronic donor levels in stannic oxide crystals", J. Appl. Phys. 44 (1973) 4618
31. C.G. van de Walle, "Hydrogen as a cause of doping in zinc oxide", Phys. Rev. Lett 85 (2000) 1012
32. Çetin Kiliç, Alex Zunger, "*n*-type doping of oxides by hydrogen", Appl. Phys.

Lett. 81 (2002) 73

33. M.H. Suhail, G. Mohan Rao, S. Mohan, "dc reactive magnetron sputtering of titanium - structural and optical characterization of TiO_2 films", J. Appl. Phys. 71 (1992) 1421
34. J. Tauc, R. Grigorovich, A. Vancu, "Optical properties and electronic structure of amorphous germanium", Phys. Stat. Sol. 15 (1966) 627
35. G.E. Jellison, M.F. Modine, Appl. Phys. Rev. Letts. 69 (1996) 415
36. A. Fontcuberta i Morral, P. Roca i Cabarrocas, C. Clerc, "Structure and hydrogen content of polymorphous silicon thin films studied by spectroscopic ellipsometry and nuclear measurements", Phys. Rev. B 69 (2004) 125307
37. H. Aguas, V. Silva, E. Fortunato, S. Lebib, P. Roca i Cabarrocas, I. Ferreira, L. Guimarães, R. Martins, "Large area deposition of polymorphous silicon by plasma enhanced chemical vapor deposition at 27.12 MHz and 13.56 MHz", Jpn. J. Appl. Phys. 42 (2003) 4935
38. M. Schubert, "Another century of ellipsometry", Ann. Phys. (Leipzig), 15 (2006) 480
39. T. Nambara, K. Yoshida, L. Miao, S. Tanemura, N. Tanaka, ''Preparation of strain-included rutile titanium oxide thin films and influence of the strain upon optical properties", Thin Solid Films 515 (2007) 3096
40. N. Popovici, E. Jimenez, R.C. da Silva, W.R. Branford, L.F. Cohen, and O. Conde, ''Optical and magnetic properties of Co-doped TiO_2 thin films grown by pulsed laser deposition'', J. Non-Cryst. Solids 352 (2006) 1486.
41. F. Zhang, G.K. Wolf, X. Wang, X. Liu, "Surface properties of silver doped titanium oxide films", Surf. & Coat. Technol. 148 (2001) 65
42. X. Lai, Q. Guo, B.K. Min, D.W. Goodman, "Synthesis and characterization of titania films on Mo(1 1 0)", Surf. Sci. 487 (2001) 1
43. F. Moudler, W.F. Stickle. P.E. Sobol, K.D. Bomben, Handbook of X-ray Photoelectron Spectroscopy, Perkin-Elmer, Eden Praitie, MN, 1992
44. J.R. Neal, A.J. Behan, R.M. Ibrahim, H.J. Blythe, M. Ziese, A.M. Fox, G.A. Gehring, "Room-temperature magneto-optics of ferromagnetic transition-metal-doped ZnO thin films", Phys. Rev. Lett. 96 (2006) 197208
45. J.M.D. Coey, "Dilute magnetic oxides", Current Opinion in Sol. State and Mater. Sci. 10 (2006) 83